



**UNIVERSITY OF NAIROBI**

**FABRICATION AND CHARACTERISATION OF NB:TIO<sub>2</sub> THIN FILM FOR  
HYDROGEN GAS SENSING APPLICATION**

**BY**

**JOSEPHAT OKWORO MOGUSU**  
I56/67237/2013

A Thesis Submitted for Examination in Partial Fulfilment of the Requirement  
for Award of the Master of Science Degree in Physics of the University of  
Nairobi

June 2021

## DECLARATION

---

I declare that this thesis is my original work and has not been submitted elsewhere for examination, award of a degree or publication. Where other people's work or my work has been used, this has been properly acknowledged and referenced in accordance with the University of Nairobi requirements.



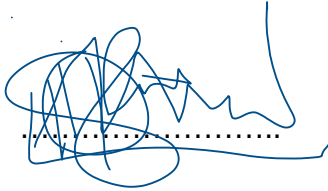


Signed....

Date...22/05/2021.....

Mr Josephat O. Mogusu  
I56/67237/2013  
Department of Physics,  
School of Physical Sciences  
University of Nairobi

This thesis is submitted with our approval as university supervisors:

	<b>Signature</b>	<b>Date</b>
Prof. Robinson J. Musembi Department of Physics University of Nairobi P.O Box 30197-00100 Nairobi Kenya siafu2001@gmail.com	 .....	26/05/2021.
Prof. Francis W. Nyongesa Department of Physics University of Nairobi P.O Box 30197-00100 Nairobi Kenya fnyongesa@uonbi.ac.ke		27/05/21...
Dr Alex A. Ogacho Department of Physics University of Nairobi P.O Box 30197-00100 ogacho@uonbi.ac.ke	 .....	27/05/2021

## **DEDICATION**

---

---

To my late mum Annah Mogusu, your strong sense of purpose, persistence and determination in life has been my greatest inspiration. My family, lovely wife Rhoda, our children, Lucy, Angela, Ann and Harrison, you allowed me to get out of my comfort zone so that I can make this significant step toward my true destiny. Also to all the people who have a desire to leave a significant mark in their generation; those who yearn to improve their lives and make a contribution to others lives.

## ACKNOWLEDGEMENT

---

I take this opportunity to recognise and thank the entire Department of Physics of the University of Nairobi for the guidance and the enabling environment that was provided to me. I could not have found better supervisors than Prof. Robinson Musembi, Prof Francis Nyongesa (Chairman, Department of physics) and Dr Alex Ogacho, I gratefully appreciate your efforts for tirelessly going through this work by reading and recommending useful corrections, you were quick, clear, and precise in your duty.

Thankfully acknowledged is the High Purity Chemicals™ for delivering to us the ceramic materials that were mainly used in this work, I appreciate the quality and timely delivery. I wish also to recognise in a special way the Condensed Matter group laboratory senior technologist, Mr Boniface Muthoka for the excellent guidance in handling and using laboratory equipment. I also mention and gratefully thank the National Commission for Science, Technology and Innovation (NACOSTI) of Kenya for their generous partial scholarship that greatly facilitated this project to its conclusion. I equally thank my employer, the Teachers Service Commission (TSC) of Kenya for granting me a study leave with pay.

To my colleagues during the tenure of research, you are my hero. We discussed and consulted amongst ourselves. You inspired and encouraged me throughout. Gratefully thanked are : Dr Victor Odari, Dr Charles Opiyo, and Dr John Nguu, while you were pursuing your doctoral studies, you mentored and motivated me. Ms Sheila Bisachi, Madam Hellen Sisia together with Sister Mary Taabu, we were together, you did your part during our studies. Mr Edwin Mwabezi and Mr Isaac Obegi, in a special way ensured I pushed on even when it looked bleak on my side. God bless you all my colleagues, you are worthy friends.

## ABSTRACT

---

A gas sensor is a selective device used in monitoring the presence or concentration level of a particular gas in the ambient atmosphere. Gas sensors operate on the principle which is anchored on any of the following three classifications, that is, spectroscopic, optical, and solid-state gas sensing methods. In spectroscopic techniques, the gas sensor is based on basic gas properties such as molecular mass or vibration spectrum, while for optical gas sensors; measurements of the absorption spectra are involved. Solid-state gas sensors apply the fact that there is a change in the electrical properties of a sensing material whenever there is exposure to gas.

Data collected on hydrogen sensors indicate that all the sensors have a low response time and are less sensitive to respond to even very low leakages of hydrogen. This work was prompted by the fact that there is continued research and study of new gas sensing materials, and therefore a likelihood in improvement in terms of response to the gas sensing properties as well as widen the choice and variety of hydrogen gas sensors fabricated using different types of materials.

Thin films of Nb:TiO<sub>2</sub> for gas sensing applications have been deposited using radio frequency (RF) magnetron sputtering. The samples were deposited at different partial pressures and sputtering power. The objectives were to analyse the optical, electrical and gas sensing properties of the thin films.

The general results on optical and electrical properties of pure TiO<sub>2</sub> and doped 2% wt Nb: TiO<sub>2</sub> and 4% wt Nb: TiO<sub>2</sub> have shown the different amount of thin-film transmittance depending on deposition conditions. The increase in partial pressure has been observed to cause a decrease in transmittance in doped TiO<sub>2</sub>, which has been attributed to competition for oxygen molecules between TiO<sub>2</sub> and NbO phase. The deposition power has also been observed to give similar results in terms of transmittance, this is because at lower power a thinner film forms while at a higher deposition power a thicker film is formed thus resulting in to decrease in transmittance. The amount of doping influences the number of free electrons and thus influencing the optical and electrical properties of thin films. The band gaps for the three types of thin films were observed to vary depending on the deposition conditions. The drop in bandgap after the post-deposition annealing was observed and is fact attributed to improved crystallinity due to an increase in electrically activated charge carriers. Finally, the sensing capability of the thin film device has been observed to improve with annealing, a factor that has been attributed to the crystallinity and charge carriers

## TABLE OF CONTENTS

<b>DECLARATION.....</b>	<b>i</b>
<b>ABSTRACT.....</b>	<b>ii</b>
<b>TABLE OF CONTENTS .....</b>	<b>v</b>
<b>LIST OF TABLES .....</b>	<b>viii</b>
<b>LIST OF FIGURES .....</b>	<b>ix</b>
<b>LIST ABBREVIATIONS AND SYMBOLS.....</b>	<b>x</b>
<b>FORMULAE OF CHEMICAL COMPOUNDS .....</b>	<b>xi</b>
<b>CHAPTER ONE: INTRODUCTION .....</b>	<b>1</b>
1.1 Background of study .....	1
1.2 Statement of the problem. ....	4
1.3 Objectives.....	4
1.3.1 Goal .....	4
1.3.2 Specific objectives .....	5
1.4. The significance of the study. ....	5
1.5 Justification .....	5
<b>CHAPTER TWO: LITERATURE REVIEW.....</b>	<b>7</b>
2.1. Overview of hydrogen gas sensors.....	7
2.2 Types of gas sensors.....	8
a) Catalytic bead sensors .....	8
b) Electrochemical sensors .....	8
c) The resistive palladium alloy sensor .....	8
d) Metal oxide semiconductor (SMO) gas sensors.....	9
2.3 The properties of TiO <sub>2</sub> semiconductor .....	15
2.4 Phases of titanium dioxide .....	17
2.5 Effects of doping of titanium dioxide .....	17
2.6 Thin films .....	20
2.7 Thin film deposition techniques .....	21
(a) The chemical deposition method .....	21
(b) Chemical vapour deposition (CVD) .....	21
(c) Plasma enhanced chemical vapour deposition (PEVCD).....	21
(d) The atomic layer deposition (ALD) method.....	22
(e) The sol- gel method .....	22

(f)	Physical vapour deposition .....	22
(g)	Molecular beam epitaxy (MBE) .....	22
(h)	The pulsed laser deposition ( PLD) .....	22
(i)	Thermal evaporation method .....	23
(j)	Sputtering method.....	23
<b>CHAPTER THREE: THEORY .....</b>	<b>24</b>	
3.0	Theory for thin film characterization and analysis.....	24
3.1	Optical properties .....	24
3.1.1	Optical reflectance .....	24
3.1.2	Optical transmittance .....	24
3.1.3	Tauc Optical band gap .....	25
3.1.4	Extinction coefficient, refractive index and absorption coefficient.....	25
3.2	Electrical properties.....	26
3.2.2	The hot -probe technique .....	26
3.2.3	The Hall Effect measurement .....	26
3.2.4	The 4- point probe technique .....	26
<b>CHAPTER FOUR: METHODOLOGY .....</b>	<b>29</b>	
4.1.	Sample preparation.....	29
4.1.1.	Substrate preparation .....	29
4.1.2.	Varied Parameters .....	29
4.2.	Thin film deposition .....	29
4.3	Properties of the thin films .....	30
4.3.1	Optical measurements of the thin film.....	30
4.3.1	Electrical properties measurements of the thin film .....	30
4.4	Gas sensing properties measurement .....	31
<b>CHAPTER FIVE: RESULTS AND DISCUSSIONS .....</b>	<b>33</b>	
5.1	Introduction .....	33
5.2	Optical properties of Nb doped TiO <sub>2</sub> thin films.....	33
5.2.1	Influence of variations in deposition pressure on transmittance .....	33
5.2.2.	Influence of variations in deposition power in transmittance.....	35
5.2.3.	Influence of niobium doping on transmittance.....	38
5.2.4.	Influence of annealing on optical transmittance.....	38
5.3.	Optical band gap of the thin films .....	41

5.3.1 Optical band gap for as-deposited thin films .....	41
5.3.2. Optical band gaps for the post annealed (450°C) for the thin films .....	42
5.4. Electrical properties of pure and doped TiO <sub>2</sub> thin films .....	43
5.4.1. Electrical properties of the thin films as-deposited .....	43
5.4.2. Electrical properties of pure and TiO <sub>2</sub> thin films as annealed .....	44
5.4.3. Comparison of electrical resistivity of the films as deposited and as annealed .....	44
5.5 Gas sensing properties.....	45
5.5.1 Influence of Deposition pressure on the gas sensing properties.....	45
5.5.2 Influence of Deposition power on the gas sensing properties .....	47
5.5.3 Influence of Niobium doping on the gas sensing properties of TiO <sub>2</sub> thin films.....	49
5.5.4 Influence of annealing temperatures on the gas sensing properties .....	50
<b>CHAPTER 6: CONCLUSION AND RECOMMENDATIONS .....</b>	<b>52</b>
6.1 Conclusion.....	52
6.2 Recommendations .....	53
<b>REFERENCES.....</b>	<b>54</b>



## LIST OF TABLES

---

---

Table 4.1: Sputter deposition parameters.....	29
Table 5.1: Comparison of band gaps as annealed and as-deposited.....	42
Table 5.2: Summary of the electrical properties as- deposited.....	43
Table 5.4: Summary of electrical properties for samples annealed at 450 °C.....	44
Table 5.5: The summary of the sheet resistance for the as-deposited and as annealed.....	44

## LIST OF FIGURES

---

---

Figure 2.1: Acoustic gas sensor schematic .....	10
Figure 2.2: Schematic diagram of a Schottky diode sensor.....	11
Figure 2.3: A schematic of MOS capacitor sensor .....	12
Figure 2.4: schematic of a MOSFET sensor .....	13
Figure 3.1: Schematic of 4- point probe configuration.....	27
Figure 4.1: The lab assembled gas sensing unit.....	31
Figure 5.1: Variations in the transmittance spectra for the TiO <sub>2</sub> thin films at different deposition pressure.....	34
Figure 5.2: The transmittance spectra for the thin films deposited at various RF power. ....	37
Figure 5.3: The transmittance spectra for pure and Nb-doped TiO <sub>2</sub> thin films deposited.....	38
Figure 5.4: The transmittance spectra for the thin films as-deposited and annealed.....	40
Figure 5.5: The Band gap curves for as-deposited thin films as deposited .....	41
Figure 5.6: Band gap curves for the post annealed films.....	42

## LIST ABBREVIATIONS AND SYMBOLS

---

A	Absorption coefficient
Cr	Chromium
E <sub>g</sub>	Optical band gap
eV	Electron volts
HCl	Hydrochloric acid
Nb	Niobium
NIR	Near-infrared
O <sub>3</sub>	Ozone
Pb	Lead
PID	Proportional Integral Derivative
PKT	Packets
Ppm	Parts per million
Pt	Platinum
RF	Radio Frequency
RRAM	Resistive Random Access Memory
TCO	Transparent Conducting Oxide
UV	Ultraviolet
VIS	Visible

## FORMULAE OF CHEMICAL COMPOUNDS

---

$\text{CH}_3\text{OH}$	Methanol
$\text{CO}_2$	Carbon dioxide
$\text{Fe}_2\text{O}_3$	Iron (iii) oxide
$\text{H}_2\text{O}$	Water
$\text{O}_2$	Oxygen
$\text{NO}$	Nitrogen monoxide
$\text{SnO}_2$	Tin (IV) oxide
$\text{SrTiO}_3$	Strontium titanate
$\text{V}_2\text{O}_3$	Vanadium trioxide
$\text{WO}_3$	Tungsten trioxide
$\text{ZnO}$	Zinc oxide

## CHAPTER ONE: INTRODUCTION

---

### 1.1 Background of the study

The devices used in the detections of the existence of gas in domestic, laboratories, and industrial environment, for the simple purpose of monitoring toxic and combustible gases as a preventive measure, are called gas sensors (Wei- Cheng *et al.*, 2013). These gadgets have been given a great attention in research activities in the last few years for diverse usage in various areas, such as alcohol level breath-tests/ breathalyser (Yang *et al.*, 2009; Bihar *et al.*, 2016; Barnett *et al.*, 2017), environmental monitoring (Rossi and Brunelli, 2012; Novikov *et al.*, 2016; Yang and Deng, 2019), indoor/ outdoor air quality (Prajapati *et al.*, 2017; Arroyo *et al.*, 2020), workplace health and safety (Kanaparthi and Singh, 2020; Thomas *et al.*, 2018), and homeland security (Rout and Roy, 2016; Sathish *et al.*, 2017). The gas sensors form essential components in contemporary electronic systems as a crossing point with the environment for monitoring gas molecules, identification, and bringing together. These days, data from environmental detection devices is vital in many scientific disciplines, and technology particularly for safety reasons, such as those deployed in environmental monitoring, industrial process monitoring, and the automobile industry (Claudio *et al.*, 2012; Ghosh *et al.*, 2019; Nazemi *et al.*, 2019; Poloju *et al.*, 2018).

The research work being reported in this thesis was devoted to hydrogen gas detection being among the many gases that are of interest in research in the recent years (Zhu and Zeng, 2017; Poloju *et al.*, 2018). Hydrogen is highly inflammable in the air at a wide range (4-75%) by volume, but if properly packaged, it can act as a very important alternative source of clean energy (Chomkitich *et al.*, 2012; Hames *et al.*, 2018). The global concern on climate change due to environmental pollution by fossil fuels considers hydrogen gas energy source as one of the best alternative clean energy for the novel transportation scenario and hydrogen derived power- sources based on fuel cells. As a fact, hydrogen is an explosive gas that can explode in ambient air at a concentration as low as 4% vol. (Arndt and Simon, 2001). In recent years, Hydrogen has steadily started to emerge as a possible alternative fuel source to supplement mineral fossil fuels. It is important to note at this juncture, that hydrogen-based fuel cells, founded on various technologies, is the technique by which energy is obtained from the reaction of hydrogen and oxygen gases within the fuel cell with by product being water as exhaust material which is a non-pollutant (Arndt and Simon, 2001).

The consumer industry for hydrogen fuel cells is based on three large market segments namely: the portable fuel cells (Lalchand *et al.*, 2014), the stationary or residential fuel cells (Ghenai *et al.*, 2020), and the automotive fuel cells (Jacobson *et al.*, 2005; Wiebe, *et al.*, 2020). Two types of sensors are required for these types of fuel cells depending on purpose of usage; first to monitor the quality of the hydrogen feed gas, and then secondly and more important sensor systems for leak detection. Hydrogen fuel cells are an emerging technology and consequently the codes and standards for the fuel cells and the sensors supporting the fuel cells are still in their nascent stages. Sensor standards and specifications for these applications are still being written, with no specific standard yet passed for use. Hydrogen gas is odourless, colourless, and tasteless, it cannot be distinguished by the human sense of smell (Xu *et al.*, 2020). The hydrogen gas has a low ignition temperature as well as a wide flammable range making it easily inflammable and explosive. It is in this regard that, rapid and accurate detection system is necessary during the manufacturing, stowage, and use of hydrogen (Lalchand *et al.*, 2014). When it is compared with domestic natural gas, sulphur-containing mercaptan gas are introduced to alert the consumer of possible gas leakage (Sun *et al.*, 2020), but this approach is not advisable in case of hydrogen, given that such add-ons can poison the fuel cell catalyst (platinum) and hydrogen sensors are needed to monitor the environment around the fuel cell for hydrogen leaks. The human nose is commonly used for natural gas detection, as it is a remarkably reliable, superb low-level detection sensor. Hydrogen leak-detection sensors differ in that these sensors must detect over the general level of ambient hydrogen levels available in the detection environment. For example, automobile lead-acid batteries evolve hydrogen routinely and for a garage-based sensor, a sensor must be able to discriminate from certain level in parts per million in ambient sources of hydrogen and those which will be generated by a hydrogen leak. Once leakage has taken place, suppression of hydrogen gas is difficult since it diffuses readily through most materials due to its intrinsic property of being the lightest gas. As a result, there will always be hydrogen gas presence in the ambient environment, if hydrogen is present in a container or if the hydrogen has evolved (Oleg *et al.*, 2008).

In order to fabricate a commercially viable hydrogen gas leak detector the following factors need to be put into consideration: redundant arrays of multiplexed sensors, selectivity to avoid false alarms; autonomous integrated fuel cell shutoff/venting measures; dependable sensing, calibration standards, and self-testing. It is a standard practise to have in place two type of sensors for leak detection, which serve two purposes: one to detect the presence of the gas and a second for alarm sensor which should be triggered when the 50% of the Lower Explosive

Limit (LEL) of 4 % hydrogen in air is reached. In our modern day society, hydrogen gas consumption is becoming common place and it is critical to have leak detection system in place. Places where large quantities of such gas are found maybe in suburban centres, fuelling stations, welding garages, and automotive repair shops (Adamyan *et al.*, 2008).

Three-dimensional detection of hydrogen gas leak requires a detector element on a probe analogous to comparable leak-detection methods. The sensor element itself must be a short response time to avert operator fatigue, be able to detect down to 1000 ppm range, and larger upper detection limit as a necessity, depending on the usage. In addition, there is a necessity to have a leakage detector that is discriminatory and ambient autonomous (Seham *et al.*, 2019), for example, a leakage sensor enclosed argon that can function accurately, this may be essential technique to prevent ignition of a compressed gas leak.

In this work, Niobium (Nb) doped Titanium dioxide (TiO<sub>2</sub>) thin films were used for fabricating hydrogen gas sensor. In the last few years, a number of materials have been used to fabricate solid-state gas sensors, among these materials, semiconductor metal oxides have dominated the materials used for the fabrication of the gas sensors (Dey, 2018). The semiconductor metal oxide gas sensors may also be known as semiconductor gas sensors. Some of the materials previously studied to fabricate the semiconductor gas sensors include SnO<sub>2</sub> (Oyabo, 1982; Wen *et al.*, 2009), ZnO (Boccuzzi *et al.*, 1992), WO<sub>3</sub> (Lin *et al.*, 1994), SrTiO<sub>3</sub> (Hu *et al.*, 2004), V<sub>2</sub>O<sub>5</sub> (Schillini *et al.*, 1994), Fe<sub>2</sub>O<sub>3</sub> and TiO<sub>2</sub> (Schillini *et al.*, 1994; Dey, 2018). For these semiconductor gas sensors, the detection indicator is founded on the alteration of the material's resistivity after gas contact. The sensitivities of the sensor devices are usually high at temperatures ranging between 200°C to 800°C as this temperature range is in the same spectrum to the optimum conductivity of semiconductors.

The material proposed in this research work was selected because prior researchers had shown that Nb doping in TiO<sub>2</sub> modifies the microstructure of TiO<sub>2</sub> by influencing the grain size growth and therefore resulting in a modification in the conductivity of the resultant material (Sukon *et al.*, 2011). In the prior literature work, a number of techniques have been described for the deposition of TiO<sub>2</sub> thin films, these includes and not limited to sputtering (Alexandrov, *et al.*, 1996), chemical vapour deposition (Rausch and Burte, 1993; Zhang and Griffin, 1995), screen printing (Bach *et al.*, 1998; Marcos, *et al.*, 2008), evaporation (Grahm *et al.*, 1998; Rao and Mohan, 1990), sol-gel method (Kim *et al.*, 2006), tape-casting (Chao and Dogan, 2011), laser

chemical vapour deposition (LCVD) (Gao *et al.*, 2012; Guo *et al.*, 2013), and spray pyrolysis (Oja *et al.*, 2006).

In this research, Nb doped TiO<sub>2</sub> thin films were prepared by vacuum radio frequency (RF) magnetron sputtering deposition method. The deposition method chosen has the following advantages over other coating techniques; low substrate temperatures are possible during deposition, good substrates adhesion of the thin film. Other factors are formation of a uniform thin film with homogeneous thickness and the ability of formation of compact thin film, as well as ease of co-deposition of different materials to form alloys, and compounds materials with possibility of varying the vapour pressures (Angelats-Silva, 2006).

## **1.2 Statement of the problem.**

Fossil fuel currently is the main source of energy worldwide despite the environmental consequences associated with them. The scientist has estimated that one time in the future they will get depleted and therefore it is important to search for an alternative source of energy during this grace period while they are available and the climatic conditions are not yet severe. Several alternative sources of energy are being mulled as possible candidates that can occupy the gap which will be left by the fossil fuel once they get depleted. Hydrogen fuel cells are a possibility and seem to be having an emerging market niche, and therefore standards and codes for these cells are still being developed, similarly, sensor specifications are still being researched. The hydrogen sensors are already in use in the market, but optimisation of a hydrogen sensor or sensor suitable to respond quickly with short reaction time to sensing requirements for fuel cells is still ongoing due to the numerous challenges being faced. Data collected on hydrogen sensors indicate that all the sensors have a low response time (8-30 seconds), which is not the expected duty cycle needed for most applications. Also noted is the lack of a more sensitive gas sensor that can respond to even very low leakage of hydrogen. It is also a fact that the maturity and specialisation of these sensors will also necessitate considerable yet realistic cost reductions, as well as a better description from the emerging fuel cell market for the probable duty cycle loads, hydrogen fuel stream pressures, flow rates, and configuration.

## **1.3 Objectives**

### **1.3.1 Goal**



The main objective of the work was to study the properties of Niobium (Nb) doped Titanium dioxide (TiO<sub>2</sub>) thin films deposited by RF sputtering technique to be used as hydrogen gas sensor.

### ***1.3.2 Specific objectives***

1. To analyse the optical properties of niobium (Nb) doped Titanium dioxide (TiO<sub>2</sub>) thin films deposited at different partial pressure and sputtering power.
2. To investigate the electrical properties of Nb doped TiO<sub>2</sub> thin films deposited at different partial pressure and sputtering power.
3. To determine the gas sensing properties of Nb doped TiO<sub>2</sub> thin films deposited at different partial pressure and sputtering power.

### **1.4. The significance of the study.**

It obvious from data collected on hydrogen sensors indicate that all the sensors have a low response time (8-30 seconds), which is not the expected duty cycle for most application. Also noted is the lack of a more sensitive gas sensor that can respond to even very low leakage of hydrogen. It is also a fact that the as this model of the sensor develops and gets highly optimised, it will be necessary to achieve some considerable and realistic cost reduction, as well as a better description from the emerging fuel cell market for the probable duty cycle loads, flow rates, hydrogen fuel stream pressures, and composition.

The continued research and study of new gas detection materials, as greater milestones are achieved there is a likelihood of improvement in terms of response to the gas sensing properties as well as widen the choice and variety of hydrogen gas sensors fabricated using a different type of materials.

The significance of materials design in innovating gas detection device is demonstrated by taking a semiconductor gas sensor as an analogy. By some innovations, the existing devices can be made more intelligent and more quantitative, which is an essential step for the further advancement of gas sensor technology. Therefore, new gas sensors for future markets can arise from the moulding of the existing gas sensor performances in realistic operational conditions utilizing a combination of spectroscopic and phenomenological techniques. Intrinsic properties of selectivity, sensitivity, and stability, which are limiting factors to the wide application of the current gas sensors still need to be addressed further.

### **1.5 Justification**

The most important characteristic of TiO<sub>2</sub> in this research work is that being a semiconducting oxide, it has the ability upon gas adsorption to change its electrical conductivity, and this change is utilised as a signature of detection when fabricating a gas sensor. The Titanium dioxide thin films have distinct characteristics at two different temperatures: At elevated temperature, Titanium dioxide thin films can be used as a thermodynamically controlled bulk defects sensor to determine gas over a large range of partial pressures, while secondly, at low temperature, as in our case, the addition of dopants like Nb and Pt. leads to high gas sensitivity and then tested widely for the sensitivity of a variety of gas.

Doping TiO<sub>2</sub> with Niobium results in modification of the pristine material and leads to a new structurally different material with different characteristics from the pure TiO<sub>2</sub> material. The same way, the levels of doping vary the characteristics of the material. Different deposition condition results in a material with different characteristics to be investigated. Since TiO<sub>2</sub> sensor materials are already in use and it is a fact that sensitivity among other qualities of sensors remains a challenge in the market, this research will dwell on studying doped materials at different percentage, and changing the deposition conditions of sensor material to come up with a more sensitive sensor.

## CHAPTER TWO: LITERATURE REVIEW

---

### 2.1. Overview of hydrogen gas sensors.

The gas sensor may be described as a selective device used in monitoring the existence of or establishing the concentration level of a particular gas in the ambient atmosphere. The working principle is founded on the changes in potential difference by changing resistivity of the material used in fabricating the sensor, this is usually triggered when the concentration of a particular gas being monitored exceeds a certain threshold value, and the potential difference is then measured as output voltage. Depending on the calibrated output voltage value, the type and its percentage presence in ambient of the gas can be estimated (Kumar *et al.*, 2015; Li *et al.*, 2018).

At present, gas sensors can be classified into three broad categories which include: solid-state gas sensor (Korotcenkov, 2007), spectroscopic gas sensor (Kassa-Baghdouche, 2020) or optical gas sensor (Meixner *et al.*, 1995). The vibrational spectrum of the target gas and, or the direct analysis of the molecular mass of a particular gas forms the basic principle of spectroscopic gas sensors. These sensors have a good precision measurement capability because molecular mass of a gas is an intrinsic property of the particular gas being measured, the best example in this class of gas detection devices are the mass chromatography gas sensor and the mass spectrograph gas sensor. Lastly, the optical sensors are based on the principle of light interaction with target material, absorption takes place and the device measures the absorption spectra. This kind of sensor is bulk and composed of a complex system which has a monochromator which acts as excitation source and an optical detector unit for the analysis of the absorbed spectra (Meixner *et al.*, 1995). Apparently, the spectroscopic and optical types of gas sensors are costly for domestic application and occasionally difficult to actualise in limited spacing such as the automotive bonnet, nonetheless, the so-called solid-state sensors present remarkable comparative advantage due to their short reaction time on gas exposure, less intricate implementation and inexpensive to acquire and mount (Woetsman *et al.*, 1995). Moreover, the traditional methods that are used for gas sensing do apply diverse technologies that result in different categories of gas sensors. Correspondingly, some of these procedures are known to give rise to bulky sensors, slow in response, and in addition, necessitate elevated temperatures and operational power for use (Haoshuang *et al.*, 2012). An ideal gas sensor will have such qualities as being of small size, low power consumption, low operation temperature, short reaction time, compactness and permit in-situ monitoring. The commercially existing and typically used gas sensor devices mainly for hydrogen detection and some other reducing gases

may fall under any of the stated groupings (Zhu and Zeng, 2017; Kumar *et al.*, 2015; Li *et al.*, 2018).

## **2.2 Types of gas sensor**

### ***a) Catalytic bead sensor***

The catalytic bead detector typically comprise two beads that enclose a wire that functions at high temperatures, usually approximately 450°C (Han *et al.*, 2007; Suehiro *et al.*, 2007). The two beads are usually not fabricated the same one, the bead is insulated such that reaction cannot take place when it comes into contact with the target gas, whereas the other bead is coated with a thin film of a catalyst so that its reaction response is amplified in the presence of gas molecules. These beads are located on the separate ends of a Wheatstone bridge circuit (De Marcellis, *et al.*, 2013). In the presence of a gas, that is, hydrogen, there is no considerable effect on the insulated bead, but there is a substantial effect registered for the other catalysed bead. The high temperature will ensure an augmentation in the bridge signal which is the sensor (Han *et al.*, 2007; Suehiro *et al.*, 2007). A pellistor coil of Pt. wire can be enveloped in a bead working at temperatures between 800°C and 1000°C. This catalytic technology is utilised by making variations for 1% to 5% of hydrogen detection. Generally, for these sensors, the control unit, together with the sensing units results in a cost of upwards of US\$1700. The response time is low at around 10 to 30 seconds (Han *et al.*, 2007; Suehiro *et al.*, 2007; Braus *et al.*, 2013).

### ***b) Electrochemical sensors***

The electrochemical sensors are composed of duo electrodes, one which acts as the cathode and the other anode. In between the electrodes, an electrolyte which is chemically sensitive is sandwiched in between. When hydrogen gas permeates inside the electrolyte, a chemical reaction will take place which will give rise to an electrical current signal. The electrical current generated is proportionate to the concentration of the gas passed and hence forms a sensor. One of the shortcomings of these types of sensors is that oxygen gas is required during the sensing process to ensure resilience to chemical reversibility. In this regard, the sensor is said not to be environmentally independent. It has a low sensitivity reaction time of between 30 to 50 seconds. Comparable to catalytic bead sensors, the electrochemical sensors are equally expensive sensors (Tao *et al.*, 2017).

### ***c) The resistive palladium alloy sensors***

The palladium alloy resistive sensor is type of devices in which the surface is made of palladium metal which acts as a catalyst to break the diatomic H-H bond of hydrogen and allow the resultant monoatomic hydrogen to diffuse into the material. The electrical resistance of the palladium coating is affected proportionately by the quantity of the monoatomic hydrogen hence the concept of gas sensing (Chadwick *et al.*, 1994; Vanotti *et al.*, 2015). These sensors are of convenient sizes, they can be used at elevated pressures, and also, they are independent of the environment such that resetting to the initial state does not require the presence of another gas. Nevertheless, when exposed to high concentrations for a prolonged duration, this may destroy the palladium coating where palladium hydride will form and thereby will potentially degrade the performance of the sensor over time (Chadwick *et al.*, 1994; Vanotti *et al.*, 2015).

#### ***d) Metal oxide semiconductor (SMO) gas sensors***

The metal oxide semiconductor gas sensors are of various types as discussed below.

##### **I. Thermoelectric gas sensors**

These gas sensors are fabricated half range surface of the nickel oxide thick film deposited with a thin film of a platinum catalyst. When exposed to air containing target gas, in this case, hydrogen, the platinum-coated surface heat up when a catalytic reaction take place exothermally. As a result, a thermoelectric voltage builds up along the cold and hot areas of the oxide film. The build-up voltage is proportional to the concentration of hydrogen in the ambient environment (Shin *et al.*, 2003; Shin *et al.*, 2004; Goto *et al.*, 2016).

##### **II. Optical gas sensors**

A good example of the optical gas sensor is the original electrochromic devices which are fabricated using tungsten oxide ( $\text{WO}_3$ ) thin films integrated with a hydrated silicon-germanium p-i-n (SiGe: H) photodetector (Lee *et al.*, 2000). This set-up combined with the palladium metal thin film which acts as a catalyst by ionising hydrogen gas, the  $\text{WO}_3$  thin film will henceforward react with a hydrogen ion and leading to change of colour from being transparent to blue. The colour change lowers the absorption range of light with other wavelengths except for the blue colour and therefore the photocurrent generated by the SiGe: H p-i-n photodetector will be lowered down thus detecting the existing hydrogen (Fine *et al.*, 2010; Nasir *et al.*, 2014). The optical gas sensors are considerably affected by humidity in the air and generally have low sensitivity as well as very poor resilience and recovery time. In the recent development, this model now involves the inclusion of optical fibre technology in hydrogen gas sensing. A fibre optic gas sensor that uses a catalyst supported tungsten trioxide ( $\text{WO}_3$ ) has been reported by Okazaki *et al.*, (2003). The tungsten thin film coating on a silica case sensor of the sensor,

when it absorbs the evanescent field, it gives the signal which is measured and this forms the basic principles of how this type of sensor works (Okazaki *et al.*, 2003; Fine *et al.*, 2010; Nasir *et al.*, 2014).

### III. Acoustic gas sensor

The acoustic sensors function in the principle of fluctuation of the acoustic wave properties analogous to the resonance frequency of the piezoelectric material due to adsorption of hydrogen gas in the sensing layer (Cheeke and Wang, 2009; Jakubik, 2011). The acoustic gas sensors are composed of the input interdigitated transducer, a semiconductor oxide thin film surface, output interdigitated transducer positioned on the surface of a piezoelectric layer as shown in Figure 2.1 below (Vellekoop, 1998).

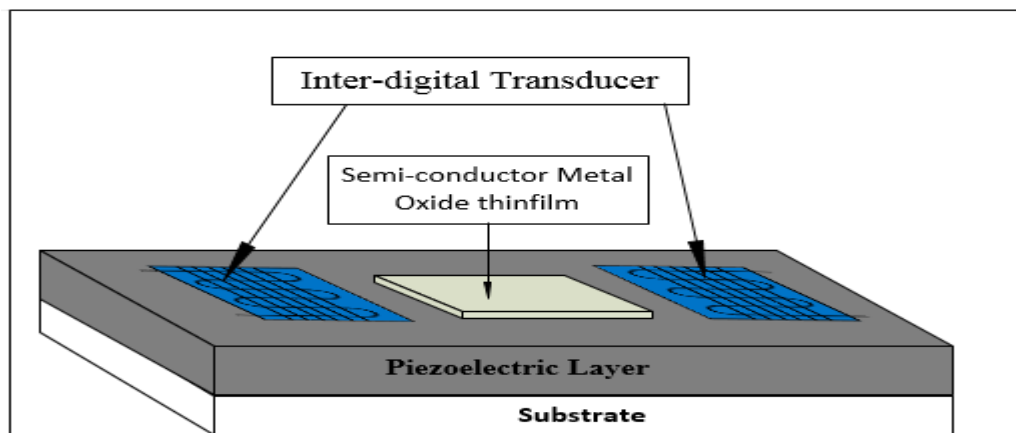


**Figure 2.1: Acoustic gas sensor schematic**

The acoustic sensor is made by two interlinking metallic electrodes similar to comb-like arrays forming what is called an interdigitated transducer. This device is then used to convert the applied electrical signal into an acoustic wave using the inverse piezoelectric effect which propagates along the surface from one to the other and then converts the acoustic signal back to an electrical signal by use of the output inter-digitalised transducer (Cheeke and Wang, 2009; Jakubik, 2011). The propagating acoustic wave signature is very sensitive to slight variations of the surface conditions on its direction of propagation; therefore any change in its signature is used to sense hydrogen gas by depositing a sensing layer made of a thin film of semiconducting oxide on top of the surface of the piezoelectric thin film layer which is between the inter-digitised layers. The presence of hydrogen gas can be detected by the frequency change on the output port of the surface acoustic wave device (Vellekoop, 1998; Cheeke and Wang, 2009; Jakubik, 2011).

### IV. Work function-based gas sensors

These are the gas sensors that operate based on the variation of the work function brought about by the presence of hydrogen gas. They are usually composed of 3- layers that are; metal/oxide/semiconductor layers. Three types of sensors result out of the multilayer configuration of these layers (Zimmer *et al.*, 2001; Pohle *et al.*, 2011; Davydovskaya *et al.*, 2013).

## V. Schottky diode sensors

The semiconductor/metal configuration type of gas sensors are called Schottky diode sensor. The sensor consists of three layers with the bottom and top electrodes acting as contacts and the active layer being made of a semiconductor material. The top electrode and the semiconductor layer which form the Schottky diode are made of materials which able to sense the gas. The front contact coated to the substrate is a metal ohmic contact electrode layer that forms a back-to-back Schottky junction structure with the semiconductor thin film or sometimes it is a gas-sensitive metal thin film layer as in figure 2.2 below (Luther *et al.*, 1999; Liu *et al.*, 2014).

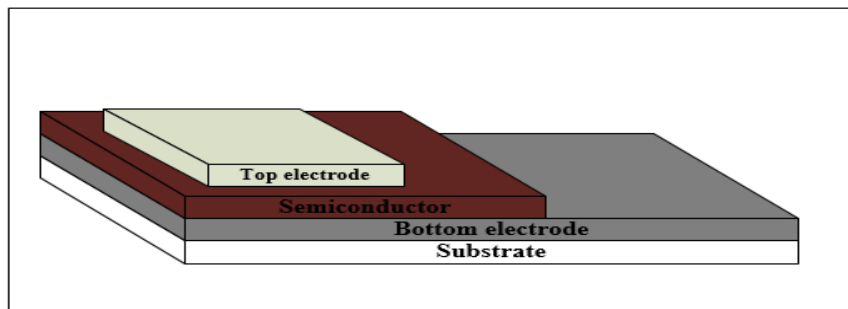


**Figure 2.2: Schematic diagram of a Schottky diode sensor**

Usually, hydrogen gas molecules will permeate and get adsorbed in the matrix of the material structure, then dissociates into hydrogen atoms in the gas-sensitive metal layer. Typically, palladium, platinum, gold, silver, copper etc. are used for the Schottky metal layer. The hydrogen atoms diffuse to form dipole layers at the interface between metal and a semiconductor, which leads to a change in the work function of the metal. The change in work function gives rise to the dissimilarity of the valence band of the semiconductor material and the work function of the metal thin film at the interface and consequently, the measured current – voltage characteristics curve will be shifted proportionally to the adsorbed hydrogen atoms, this difference is used to calculate the level of concentrations (Luther *et al.*, 1999; Liu *et al.*, 2014).

## VI. MOS capacitor sensors

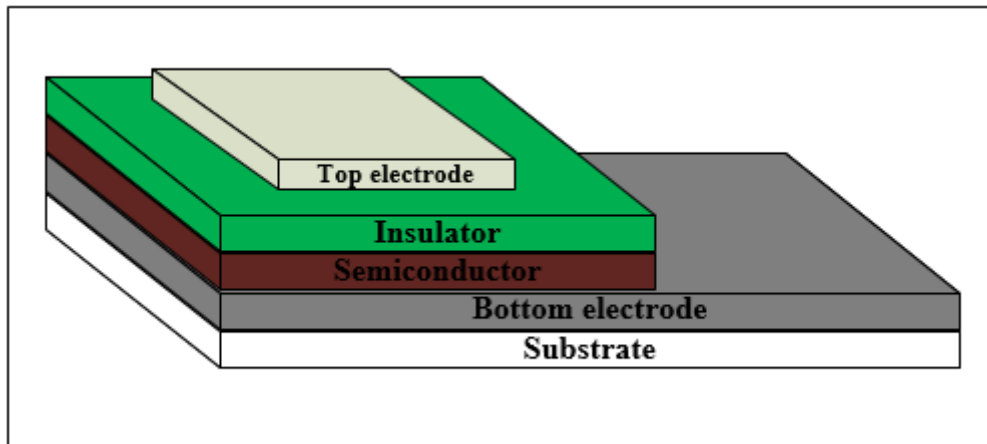


**Figure 2.3: A schematic of MOS capacitor sensor**

The Metal-Oxide-Semiconductor (MOS) type of gas sensors are mainly composed of a thick film of insulating layer coated between the metal thin film layer which acts as a gas sensitive catalyst, and the semiconductor thin film layer with duo purpose to prevent the current conduction as well as encourage built up a charge accumulation layer on both sides (figure 2.3). In an ambient atmosphere containing the dissociated hydrogen atoms when it comes into contact with the catalytic sensitive metal layer of the gas sensor, the gas diffuses into the metal/insulator interface, when capacitance-voltage (C- V) and conductance-voltage (G-V) are plotted, the results are consistent to the hydrogen concentration in the surrounding and hence acting as a sensor (Zhang *et al.*, 2014; Bagolini *et al.*, 2019).



## VII. MOSFET sensors

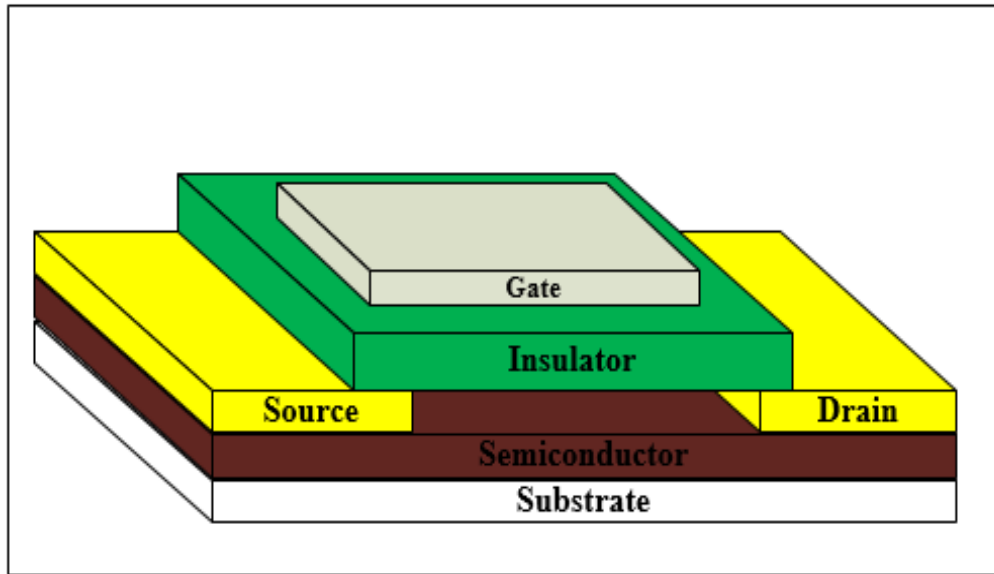


**Figure 2.4: schematic of a MOSFET sensor**

The Metal-Oxide-Semiconductor Field-Effect Transistor (MOSFET) type of gas sensors are designed with the gate (catalytic gas-sensitive metal), the drain, the source, and an insulator underlayer as shown in figure 2.4 above. If the sensor gets exposed to a hydrogen gas containing environment, the hydrogen atoms permeate to the interface between the metal and the insulator and forms a dipole layer that varies the gate voltage. When the source is grounded, the conduction between the source and the drain can be adjusted by the changes in the gate voltage. The variations on the gate voltage can be because of the change in concentration of the hydrogen gas atmosphere, which thereby will correspond to the measured voltage signal (Haugen *et al.*, 2000; Gu *et al.*, 2012).

## VIII. Resistance based semiconductor (SMO) gas sensors

In the last decade, a variety of solid-state gas sensors were designed and commercialised targeting various sectors of the market mainly for safety, automotive, process control or household applications (Noboru, 2005; Kumar *et al.*, 2015; Li *et al.*, 2018). Metal oxide semiconductors are known to be sensitive to the existence of impurities in their bulk or on their surface. This sensitivity is affected significantly by the electrical resistance of the semiconductors, as was demonstrated by Brattain and Bardeen, (1953) for Germanium. The variation of electrical properties of ZnO, when exposed to reducing gases, was first reported in

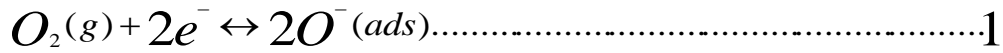
the early 1950s (Wagner, 1950). It is extensively reported that this detection mechanism by a change in electrical resistance in the case of n-type semiconducting oxides, which is linked to the existence of surface oxygen adsorbents which build up space-charge layer at the metal oxide surface (Bie *et al.*, 2007; Stamataki *et al.*, 2008; Lee *et al.*, 2010; Majumdar *et al.*, 2014). When a reaction takes in a reducing gas, the adsorbents trigger an increase in oxide conductance (Enrico *et al.*, 2001). The working principle of the resistance-based gas sensor is that when gases get adsorbed on the surface of the thin film, this leads to change in electrical sheet resistance of the material. The change in electrical sheet resistance is because when some gas species are adsorbed, this leads to the formation of a charge depletion layer affecting the movement of charge carriers from one location to another. The adsorption of oxidising gases such as nitric oxide and ozone have a tendency of increasing thin film electrical sheet resistance of the sensor. Nevertheless, reducing gases such as hydrogen or methyl alcohol cause a reduction in the adsorbed oxygen leading to a change in the electrical sheet resistance of the sensor material (Bie *et al.*, 2007; Stamataki *et al.*, 2008; Lee *et al.*, 2010; Naji Al Dahoudi, 2011).

Most researches studying the effect of adsorption and desorption properties on the surface of metal oxide semiconductors, observed a remarkable change in electrical resistance similarly as was observed by the studies on ZnO<sub>2</sub> thin films at a temperature of 300°C, (Selyama *et al.*, 1962; Lee *et al.*, 2010). A similar procedure researched on other metal oxide thin films showed an improvement in most of them being applied as gas sensors (Bie *et al.*, 2007; Stamataki *et al.*, 2008; Lee *et al.*, 2010; Naji Al Dahoudi, 2011).

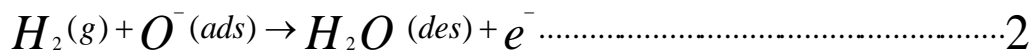
A series of research works about the sensing behaviour of these SMEs to reducing gases such as hydrogen gas have been reported, including SnO<sub>2</sub> (Wang *et al.*, 2008), ZnO (Zhu *et al.*, 2017), TiO<sub>2</sub> (Li *et al.*, 2018) Nb<sub>2</sub>O<sub>5</sub> (Rani *et al.* 2013), FeO (Song *et al.*, 2004), Fe<sub>2</sub>O<sub>3</sub> (Bandgar *et al.*, 2014) NiO (Hotovy *et al.*, 2002), Ga<sub>2</sub>O<sub>3</sub> (Ogita *et al.*, 1999) Sb<sub>2</sub>O<sub>5</sub> (Han, 2010) MoO<sub>3</sub> (Han 2010), V<sub>2</sub>O<sub>5</sub> (Han 2010), and WO<sub>3</sub> (Han 2010) which exhibit substantial dissimilarities in resistance after coming into contact with the gas. Another oxide that has shown the same properties is In<sub>2</sub>O<sub>3</sub> (Huang *et al.*, 2009).

The hydrogen gas sensor has gained a lot of interest ever since the material emerged as a vital alternative source of energy. Most materials used in hydrogen gas sensor fabrication are derived from metal oxides which most of them are cheaper when it comes to production. (Wen *et al.*, 2010). When Oxygen from the atmosphere is adsorbed on the surface of the metal oxide

thin film, MOX, in the form of various species ( $O_2^-$ ,  $O^{2-}$  and  $O^-$ ) depending on the operational temperature (Azhar *et al.* 2012).



If the gas sensor is fabricated using an n-type semiconductor, the adsorbed oxygen gas is reduced therefore decreasing the electrical sheet resistance which is caused by electrons which get trapped from the surface resulting into formation of a depletion layer on the surface. The adsorbed oxygen can be desorbed (*des*) by introducing a reducing gas, such as hydrogen, the process is as described by equation 2 below:



The process described by equation 2 above, shows that a cyclic process where the trapped electrons are replenished back to the conduction band therefore partially or fully restoring the conductivity of the thin film. The changes in electrical sheet resistance of the thin film is in this sense used to determine the concentration of reducing and oxidizing gases.

### 2.3 The properties of TiO<sub>2</sub> semiconductor

The intrinsic properties of Titanium dioxide (TiO<sub>2</sub>) have been widely studied because of its usefulness in a wide variety of applications that include: ant reflectance, dielectrics films, photocatalysis, gas sensing, protective coatings, and optical coatings (Bedikyan *et al.*, 2013). The TiO<sub>2</sub> material has also attracted much attention for application in the electronics sector, and efforts at using it as a high K- dielectric material (Kington *et al.*, 2000) as well as in resistive random-access memory (RRAM) devices have been made as an alternative to silicon oxide (Fujimoto *et al.*, 2006).

The other properties of titanium dioxide semiconductor material are photoelectric and photochemical properties. In the literature work reported by Fujishima and Honda (1972) on the photolysis of water on TiO<sub>2</sub> electrodes without an external bias, and the possibility that surface defect states may be the cause in the decomposition of water into H<sub>2</sub> and O<sub>2</sub>, gave rise to much of the early work on TiO<sub>2</sub>.

Furthermore, the photo-assisted degradation of the organic molecule has been one of the most enthusiastically applied in researches. The TiO<sub>2</sub> being a semiconductor, when it gets irradiated with sunlight, the electron-hole pair is created leading to dissociation, the charge carriers

created can drift to the surface. At this point, the adsorbed organic molecule reacts with the electron-hole pair leading to complete decomposition into CO<sub>2</sub> and H<sub>2</sub>O (Bedikyan *et al.*, 2013). The application for this mechanism ranges from wastewater purifiers, disinfection of bacterial based on properties of TiO<sub>2</sub> and use of a self-cleaning coating on car windscreens to protective coatings of marble.

The intrinsic property of the titanium oxide wide bandgap which is 3.0 eV for rutile and 3.2 eV for anatase, enables it to exhibit photocatalytic properties only under ultraviolet light irradiation, this characteristics of its bandgap has seen it acts as a good window layer material in photovoltaic applications. In fact, TiO<sub>2</sub> is widely used in the application of a dye-sensitised solar cell. As a result, TiO<sub>2</sub> forms an excellent substitute in developing equipment that can convert energy efficiently from light to electricity using dye-sensitised solar cells with the knowledge of nanoparticles since the frequently used silicon technology is demanding in machinery and in unprocessed materials, (Dakka *et al.*, 1999).

The properties of TiO<sub>2</sub> possessing a high refractive index are exploited as an antireflection coating and in beam splitters because of its high dielectric constant and refractive index (Mangrola *et al.*, 2010). Titanium dioxide is also extensively used in paints, due to its refractive ability and as a constituent of paints used to coat cars, boats, and aeroplanes. In addition, TiO<sub>2</sub> is found in several construction and building materials. The plastic industries also make use of it as a coating to absorb ultraviolet light and for enhancement of durability. TiO<sub>2</sub> has been found to possess compatibility properties with the human body; hence it is used as a biomaterial, that is as a bone substituent and reinforcing mechanical support (Cai *et al.*, 2003).

Due to its nontoxic nature, TiO<sub>2</sub> finds a safe application for domestic use and can be dispersed easily. The white colour of certain foods such as dairy products and candy, is due to the usage of TiO<sub>2</sub> as a pigment, furthermore, it is used in lending brilliance to toothpaste, in medications, as food additive and flavour enhancer in a variety of non-white foods, as well as beer and wine. TiO<sub>2</sub> is often included in many cosmetic preparations to act as an antiglare for skin products. It is also a significant component of sunscreen to attenuate the absorption of ultraviolet rays from the sun, the concentration of which determines the product is the sun protection factor.

The most important characteristic of TiO<sub>2</sub> in this research is that being a semiconducting oxide, it has the capability to change its conductivity upon gas adsorption and this change in electrical signal has enabled it to be utilised as an oxygen gas sensor for example to control air /fuel mixture in car engines (Xu *et al.*, 1993). TiO<sub>2</sub> exhibit distinct characteristics at two different

temperatures. At high temperature, TiO<sub>2</sub> can be used as a thermodynamically controlled bulk defects sensor to determine oxygen over a large range of partial pressures. At low temperature, the addition of dopants like Nb and Pt. leads to high oxygen sensitivity and then tested widely for the sensitivity of a variety of other gases (Valencie *et al.*, 2012).

#### **2.4 Phases of titanium dioxide**

It is well identified that Titania can occur in three different crystalline phases apart from the amorphous phase and orthorhombic one, it exists in brookite and two tetragonal phases, that is the anatase and rutile (Dakka *et al.*, 1999). Nevertheless, only rutile and anatase phases are exploited in the applications of TiO<sub>2</sub> and are of great research interest. For coarse-grained Titania, rutile is the only stable phase whereas anatase and brookite are metastable at all temperatures and change to rutile when annealed. However, for the case of titanium nanoparticles, the anatase and rutile stabilities are reversed due to the competition among the surface energy and transformation energy. Because of this, at small particle sizes, the anatase is more stable than the rutile structures (Mwangrola *et al.*, 2012). Anatase structure, therefore, is highly preferred over the rutile structure because of its higher electron mobility, lower dielectric constants, lower density, and lower deposition temperature, and it finds application for gas sensor applications and solar energy applications. Moreover, anatase TiO<sub>2</sub> has an indirect bandgap and possesses a bandgap value of 3.2eV-3.35eV when in a thin film state.

#### **2.5 Effects of doping of titanium dioxide**

Research on metal oxide semiconductor gas sensors is aimed at coming up with devices that will exhibit enhanced sensitivity, precise selectivity, and improved long-term stability and furthermore to be inexpensive and convenient to use. Therefore, the design for more efficient gas sensors devices has become a particularly active research field in the world as a contribution to pollution regulation for industry processes, which is a global problem, and laboratory working area as a safety measure (Moos *et al.*, 2009; Zhu *et al.*, 2017, Li *et al.*, 2018).

Gas sensing fabrication will involve developing a thin film with desirable characteristics such as high porosity for faster response, small grain size, and either low conductivity (for reducing gases) and high conductivity (for oxidising gas) in order to optimise for higher sensitivity (Raluca *et al.*, 2009). To improve or accomplish these gas sensing characteristics, the use of dopants, preparation and deposition technology for the thin film, crystal structure variation,

operation temperatures and pressure remain the key factors under study year in year out, which is a global problem, (Bochenkov and Serger, 2005; Zhu *et al.*, 2017, Li *et al.*, 2018).

Most gas sensors are mainly solid-state thin films, which can be deposited using a variety of techniques in the laboratory, such as sputtering, evaporation, electrodeposition, spray pyrolysis, anodization, sol-gel etc. A number of research have been performed to analyse the effect of dopants on the sensitivity, selectivity, and working temperature of the TiO<sub>2</sub> thin film-based gas sensors. Some of the elements such as Pb, Pt., Nb, Cu, W, Cr and Sn, used in doping TiO<sub>2</sub>, Nb and Pt-doped TiO<sub>2</sub> have exhibited promising gas sensitivity performance (Zhu *et al.*, 2017, Li *et al.*, 2018).

Sol-gel technique has been used in the deposition of pure TiO<sub>2</sub> and Nb-doped TiO<sub>2</sub> porous thin films where doping revealed an increase in conductivity as a result of the introduction of electrons into the titanium film, i.e. lattice reaction (Violeta *et al.*, 2011; Zhu *et al.*, 2017, Li *et al.*, 2018). The same research reports of a fine microstructure, (smaller grain size), which are more porous due to inhibited grain growth for the doped films. The small grain structure because of doping increased the gas sensing properties as more gas is adsorbed. Similarly described by other researchers (Anukunprasert *et al.*, 2005; Zhu *et al.*, 2017, Li *et al.*, 2018), Nb-doped TiO<sub>2</sub> at 3-5 mole % evidently hampers the anatase- to- rutile phase transition and impedes grain growth in contrast with pure TiO<sub>2</sub>. The doping improves the conductivity of TiO<sub>2</sub>, primarily in the high-temperature range where the material is most sensitive to gaseous species (Vardan *et al.*, 2013). Consequently, given the high resistivity of pure TiO<sub>2</sub>, conductivity improvement is essential for low cost gas sensing. Furthermore, the introduction of dopants greatly enhances the gas sensing performance of TiO<sub>2</sub> nanostructures.

In the work done by Sukon *et al.*, (2011), it was reported that sensitivity of Nb doped TiO<sub>2</sub> improved and the best results were observed for 4% Nb/TiO<sub>2</sub> doping and that Nb stabilised the anatase phase and retarded grain growth up to 600° C. Transition to the rutile phase in the thin film causes conductivity to decrease significantly, likely due to disruption of percolative pathways through the anatase phase. Correspondingly reported is the sensing performance of pure TiO<sub>2</sub> and doped TiO<sub>2</sub>(with noble metals) where it was observed a better response to CO gas, for doped TiO<sub>2</sub> gas sensors (Adawiya *et al.*, 2011; Zhu *et al.*, 2017, Li *et al.*, 2018).

An assortment of gas sensors founded on diverse principles have been proposed for in-situ monitoring of hydrogen gas leak (Aroutiounian, 2005; Zhu *et al.*, 2017, Li *et al.*, 2018). Owing to their simple operation, low cost of production, and excellent performances, metal oxide

semiconductor (MOS) devices have been explored primarily as hydrogen gas sensors. In particular, MOS gas sensors founded on TiO<sub>2</sub> semiconductor received special consideration due to their exceptional performance. The addition of modifiers (e.g. noble metals) or UV irradiation exposure to enhance the performance has been largely pursued (Epifani *et al.*, 2008).

Gas sensors operate on the principle which is anchored to any of the following three classifications, that is, spectroscopic, optical, and solid-state gas sensing methods. In spectroscopic techniques, the gas sensor is based on basic gas properties such as molecular mass or vibrational spectrum, while for optical gas sensors; measurements of the absorption spectra through light simulations are involved. Lastly, solid-state gas sensors apply the fact that there is a change in the electrical properties of a sensing material whenever there is exposure to a gas (Chengxiang *et al.*, 2010; Zhu *et al.*, 2017, Li *et al.*, 2018).

In this study, solid-state gas sensors are considered. There is a large variety of materials used in fabricating solid-state gas sensors; so far, the most dominant materials are those derived from metal oxides and are simply known as semiconductor gas sensors. Among the metal oxides that are studied most as gas sensor materials include SnO<sub>2</sub> (Oyabo, 1982), ZnO (Boccuzzi *et al.*, 1992), WO<sub>3</sub> (Lin *et al.*, 1994), SrTiO<sub>3</sub>, V<sub>2</sub>O<sub>5</sub> (Schillini *et al.*, 1994), Fe<sub>2</sub>O<sub>3</sub> and TiO<sub>2</sub>. For these semiconductor gas sensors, the detection indicator is founded on the alteration of material resistivity after gas contact. The sensitivities of the sensor devices are usually high at temperatures ranging from 200 °C to 800 °C as this range relates to the optimum conductivity of the semiconductors (Chengxiang *et al.*, 2010; Zhu *et al.*, 2017, Li *et al.*, 2018).

Furthermore, it is a recognised fact that the characteristic peak sensitivity usually depends on the gas to be tested, the intrinsic properties of the sensor material, or its doping. Current research on semiconductor gas sensor materials is concentrated not only on coming up with a new type of materials but also on the improvement of the characteristics of existing sensors (Comini *et al.*, 2000). Ideal case type of gas sensors are envisaged to possess high sensitivity towards chemical compounds (Ferroni *et al.*, 2001), high selectivity (low cross-sensitivity) for a particular type of gas or chemical compound (Sheilesh *et al.*, 2011), high permanence and flexibility (short reaction and recovery time), low sensitivity to humidity and temperature, high reproducibility and consistency, toughness and be able to withstand extreme conditions, possess straightforward graduation procedure and small extents (Wei-Cheng *et al.*, 2013). Most of these properties are dependent not only on the material to be used in fabrication, fabrication

procedure and the doping additives present in the oxide semiconductor material but also on the method used for their incorporation.

In this work, a doped TiO<sub>2</sub> solid-state gas sensor was used. TiO<sub>2</sub> has been chosen, due to its excellent chemical, electrical and optical properties, nontoxicity, good mechanical toughness, and high transparency in the visible region (Karunagaran *et al.*, 2005). Furthermore, it exhibits excellent photocatalytic and super-hydrophilic properties (Yu *et al.*, 2000) and is a promising material for humidity, chemical, and gas sensors, especially for organic compounds. Also, the choice has been based on its high photo corrosive resistance, efficient photocatalyst for extensive environmental applications for its strong oxidising power and high photochemical corrosiveness resistance (Weast and Selby, 1967).

In this study, TiO<sub>2</sub> was pre-doped with niobium to modify its microstructure by controlling grain growth and hence modifying its conductivity (Sukon *et al.*, 2011). The anatase to rutile phase change induced grain size growth which is expected to affect the gas response even at a lower temperature (Enrico *et al.*, 2001). The presence of small amounts of Nb in Titania leads to the change in electrical conductivity and therefore improves the gas selectivity of the sensor (Violeta *et al.*, 2012). Another critical parameter is the method of film deposition. The sputtering technique, among many other methods, was proposed, for a more stable film material and ease in controlling film thickness to optimum levels by changing sputtering time (Prabir *et al.*, 2005). Also, it's expected that deposition of the films at various partial pressures and temperatures will give a variety of gas responses.

## **2.6 Thin films**

A thin film is a layer of material ranging from a fraction of a nanometre to several micrometres in thickness (Kaiser, 2002). They are usually low dimensional materials created by condensing one by one atomic, molecular, or ionic species of matter. They differ from thick films which results from three-dimensional building up of material leading to large grains, aggregates, clusters of atoms, molecular species and ionic species (Kasier, 2002; Chengxiang *et al.*, 2010; Zhu *et al.*, 2017, Li *et al.*, 2018).

The knowledge on thin films is applied dependably in wide fields of science and technology in the application of coatings. These thin-film coatings are used to alter and improve the functioning ability of a bulk surface or substrate. In most cases, the thin film coatings do not modify the properties of the bulk material but they totally change the optical, electrical



transport and thermal properties of a surface or substrate due to the resulting surface and interface effects which considerably dominates the overall behaviour of thin films (Kaiser, 2002; Olayinka *et al.*, 2019).

The increased functionality has resulted in wide applications of thin films in electronic semiconductor device development. The semiconductor materials in thin-film form have been applied in transparent electrodes, photovoltaic devices, solar front panel displays, surface acoustic wave devices, low emissivity coatings for architectural glass, heat reflectors for advanced gazing in solar cells and finally but not least development of various gas sensors.

## **2.7 Thin film deposition techniques**

The functionality of a thin film material not only depends on texture, aesthetics, and colour which are physical appearances (Kaiser, 2002) but also will mainly depend on bulk and the surface characteristics composition, especially on the area of application where surface contact behaviour is very important. The existing external conditions also will influence the expected performance. Therefore, the functional component must satisfactorily perform the desired purposes efficiently and successfully under varied environments such as hospitals and industry without deteriorating or yielding to disastrous calamities. The properties and performance of thin films can be obtained by careful selection of proper thin-film technique. Many thin-film deposition techniques are available for use and have been categorised into two, namely, chemical and physical methods (Dleradil, 2019)

### ***(a) The chemical deposition method***

Generally, in chemical methods, fluid precursors are used which react chemically with a substrate to form a thin film. Some of the methods under this category are as follows.

### ***(b) Chemical vapour deposition (CVD)***

Chemical vapour deposition (CVD) is a chemical process in which the gaseous precursor is used. The precursor gases and the substrate are moved into a chamber. Then a chemical reaction will take place between the substrate and precursor at a high temperature until the desired thickness of a thin film is obtained on the substrate (Kempster, 1992).

### ***(c) Plasma enhanced chemical vapour deposition (PEVCD)***

In this technique, a plasma is formed in a reaction chamber. The plasma will transform the precursors into reactive ions, radicals, neutral atoms, and molecules. These atomic and molecular fragments, when they come into contact with the substrate chemical reaction ensues

that develops a solid layer on the surface of the substrate (Farid *et al.*,2018). This will require lower temperatures for the reaction to occur when compared to the CVD.

***(d) The atomic layer deposition (ALD) method***

In this method, two or more gaseous precursors are used and are permitted to react with the substrate one at a time (sequentially). This technique is a slow procedure since it is stepwise that has the advantage of working in lower temperatures and it results in conformal thin films (Titta *et al.*,2003).

***(e) The sol-gel method***

This is a technique that is between the chemical and physical processes of thin film development. A sol is a dispersion of the solid particles in a liquid where only the Brownian motions suspend the particles. A gel is a state where liquid and solid are dispersed in each other, which presents a solid network containing liquid components. Deposition techniques in sol-gel deposition include spraying method, spin coating, and dip coating (Hench and West, 1990).

***(f) Physical vapour deposition***

Physical vapour deposition involves physical techniques, mechanical and electrochemical methods are used to develop thin films. The materials to be deposited on a substrate depend on factors such as pressure, temperature and other physical conditions that are predominant. The thin films that result from these procedures are directional in nature since the particles will follow a linear path from the target to the substrate. The methods that fall under this category will include the following techniques.

***(g) Molecular beam epitaxy (MBE)***

In this process, the target materials are heated directly until they convert from solid to gaseous. Thereafter, the gaseous element will be permitted to react chemically with the substrate to grow a thin film on it (Panish., 1980). The molecular beam epitaxy combines a physical and chemical process. The purity of the resulting thin films is very high.

***(h) Pulsed laser deposition (PLD)***

The pulsed laser deposition utilises a high power of pulses of laser light which are focused on the surface of the target material in a vacuum chamber. The process results in knocking off of atoms from the target material. The atoms obtained from the target material get deposited on the substrate to form a thin film (Hiroaki *et al.*, 2016).

***(i) Thermal evaporation method***

The thermal evaporation method involves the process of resistive evaporation of the material to be deposited, the material is placed in a substrate holder which may be in the form of a boat, basket or coil, then the current at high voltage is passed to melt and evaporate the material in a vacuum chamber. The vacuum then allows the vapour particles to travel directly to the substrate where they condense back to a solid state to form a thin film (Ravish *et al.*, 2019).

***(j) Sputtering method***

This is a method in which the atoms from a target material are knocked off by the ionised sputter gas and come to rest on a substrate. Temperatures of target materials are kept low. The plasma of inert gas such as argon is used since they do not allow undesired chemical reactions to take place in the chamber. A voltage is applied between anode and cathode electrodes, it is a fast and effective method of film deposition in which a desired thin film with good adherence to the substrate is achieved. Furthermore, it permits better control of the film thickness (Tevers *et al.*, 2007)

In the process of sputtering, surface atoms from the target material are ejected from an electrode surface by momentum transfer from bombarding ions to the surface. The sputtering technique can be of numerous methods that include glow discharge sputtering, diode sputtering, reactive sputtering, bias direct current (DC) sputtering, and radio frequency (RF) sputtering.

In RF sputtering is primarily used for insulator thin films and at lower pressures. An RF potential is applied at the metal electrode placed behind the dielectric plate target (Sirgil *et al.*, 2002)

**3.0 Theory for thin-film characterization and analysis**

Characterisation is an important step in the development of better-quality materials. Some of the various analysis techniques used for thin films are discussed. This is important to evaluate the material quality of the semiconductor thin film and comprehend how diverse parameters are calculated as well as how the parameter values are interpreted in order to understand the results. The techniques used in this work are discussed in detail under this section.

**3.1 Optical properties**

**3.1.1 Optical reflectance**

Reflectance is the percentage measure of the ratio of the intensity of incident light to that of the reflected light. While using a spectrophotometer for its measurement, incident light of known wavelength is directed on the surface of a thin film and the intensity of the reflected light measured. The two intensities, that is, the incident light intensity, and reflected light intensity are compared in a reference called the reflectance, (R), as given by the equation below;

$$R = \frac{I_R}{I_0} \times 100\% \dots\dots\dots 4$$

Where,  $I_0$  and  $I_R$  are intensities of the incident and reflected beams, respectively.

**3.1.2 Optical transmittance**

The light photons from a lamp are passed through a grating or a monochromator which splits the light into selected wavelengths of beam intensity,  $I_0$  (photons/cm<sup>2</sup>), are directed at a thin film of thickness,  $d$ , constructive and destructive interference occurs and relative transmission is observed. For exact measurement of the material bandgap,  $E_g$ , photons with energies less than the bandgap do not excite electrons in the valence band to the higher states, hence are transmitted while those photons with energies greater than the bandgap, they excite the electrons in the valence band to higher energy states and therefore are absorbed. Hence transmittance is the ratio of the incident photons to the transmitted photons as given by the equation below.

$$T = \frac{I_t}{I_0} \times 100\% \dots\dots\dots 5$$

Where  $I_t$  is the intensity of the transmitted photons and  $I_0$  is the intensity of the incident photons.

**3.1.3 Tauc Optical band gap**

An optical band gap of material is defined as the energy difference between the top of the valence band and the bottom of the conduction band. The fundamental absorption that is proportional to the electron excitation from the valence band to conduction band can be used to estimate the value of optical band gap. The relationship between the absorption coefficient,  $\alpha$ , and the incident photon energy,  $h\nu$ , can be written as (Li *et. al.*, 2010).

$$\alpha h\nu = A(h\nu - E_g)^n \dots\dots\dots 6$$

where  $A$  is a constant,  $E_g$  is the optical bandgap of the material,  $h\nu$  is the photon energy,  $\alpha$  is the absorption coefficient, the index,  $n$ , defines the nature of transitions where  $n=1/2, 2, 3/2$  or  $3$  for allowed direct, indirect, forbidden direct and forbidden indirect transitions, respectively.

A graph plotted with  $(\alpha h\nu)^2$  versus  $h\nu$  or  $(\alpha h\nu)^{\frac{1}{2}}$  versus  $h\nu$  for direct or indirect bandgap respectively, will result in curves whose tangential intercept of the line to the  $h\nu$  axis gives estimated Tauc bandgap.

**3.1.4 Extinction coefficient, refractive index and absorption coefficient.**

The values for extinction coefficient, the refractive index and the absorption coefficient can be calculated from the transmittance equation;

$$T = (1 - R)^2 \exp(-\alpha d) \dots\dots\dots 7$$

Where  $R$  is the reflectance of the thin film,  $\alpha$  is the absorption coefficient, and  $d$  is the thin film thickness.

The reflectance is associated to the refractive index  $n$  and extinction coefficient  $k$  by [Heavens, 2003];

$$R = \frac{(n-1)^2 + k^2}{(n+1)^2 + k^2} \dots\dots\dots 8$$

The value of  $k$  is normally obtained using the formula [Banerjee *et al.*, 2005];

$$k = \frac{2\alpha}{4\pi} \dots\dots\dots 9$$

And

$$\lambda = \frac{hc}{E} \dots\dots\dots 10$$

Where  $h$  is Planck's constant ( $6.623 \times 10^{-34}$  Js) and  $c$  is the speed of light in a vacuum ( $2.998 \times 10^8$  m/s). The value of  $hc$  is a constant equal to 1240 eV. The extinction coefficient, refractive index and absorption coefficient were determined using these equations.

### 3.2 Electrical properties

#### 3.2.2 *The hot -probe technique*

The semiconductor conductivity can be determined using a hot probe method. In this method also known as the thermoelectric probe type, the conductivity is determined by the sign of the thermal emf or Seebeck voltage generated by a temperature gradient.

Two probes contact the sample surface; one is hot while the other is cold. Electrons will diffuse from the hot to the cold region setting up an electric field that opposes the diffusion. The electric field produces a potential detected by a voltmeter with the hot probe positive with respect to the cold probe.

#### 3.2.3 *The Hall Effect measurement*

The Hall Effect measurement technique has a wide application in the characterisation of semiconductor materials. The measurement gives resistivity, the charge carrier density carrier mobility.

#### 3.2.4 *The 4- point probe technique*

The 4 –point probe set up has four equally placed metal tips as in the figure below.

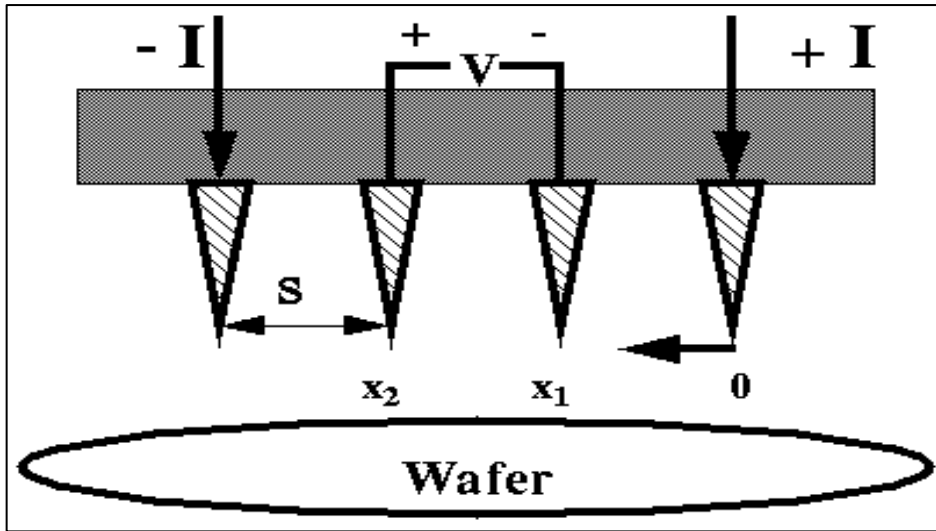


**Figure 3.1: Schematic of 4- point probe configuration**

A high impedance current source supplies current through the outer two probes and the voltage across the inner probes is measured for determination of sample resistivity.

For a thin layer sample/wafer (thickness,  $t \ll$  probe sample spacing,  $s$ ), current rings instead of spheres are obtained [Brown, 1996]. Therefore, the current area is given by the equation;

$$A=2\pi xt.....11$$

While the sheet resistance  $R_s$  is given by the equation below

$$R_s = \int_{x_1}^{x_2} \rho \frac{dx}{2\pi xt}.....12$$

Where  $\rho$  is resistivity.

From equation 12 we obtain;

$$R_s = \int_s^{2s} \frac{\rho}{2\pi xt} \frac{dx}{x} = \frac{\rho}{2\pi t} (\ln x) \Big|_s^{2s} = \frac{\rho}{2\pi t} (\ln 2).....13$$

Given that,

$R = \frac{V}{I}$ , then the sheet resistivity of the square geometric thin film is given by;

$$\rho = \frac{\pi t V}{\ln 2 I}.....14$$

This equation 14 is independent of probe distance  $s$ . In general, this equation can be expressed as,

$$\rho_s = \beta \frac{V}{I} \dots\dots\dots 15$$

Where  $\beta$  is a geometric factor and in the case of a semi-infinite thin sheet,  $\beta = 4.53$  which is just  $\frac{\pi}{\ln 2}$  from derivation. Equation 15 was then used to determine the sheet resistance of the thin films.



## CHAPTER FOUR: METHODOLOGY

### 4.1. Sample preparation

#### 4.1.1. Substrate preparation

The samples were deposited on 3.5 cm × 2.5 cm fluorine-doped tin oxide (FTO) conducting glass substrate with an average sheet resistance of 9 Ω/□ from Sigma Adrich™ Company.

The following procedure was followed in cleaning the substrate before coating; first, the samples were soaked in a soapy solution for 10 minutes while being agitated in an ultrasonic bath, after that they were rinsed using distilled water. After this process, the substrates were immersed in a beaker containing acetone and put under sonication process for another 10 minutes, followed by ethanol under the same conditions. The clean substrates were rinsed in distilled water and placed in a rack in a dustless chamber to dry. After drying, they were stored in desiccators ready for use.

#### 4.1.2. Varied Parameters

The table below indicates the parameters that were varied and those that were kept constant. The constant parameters were obtained after optimisation of the sputtering system. The optimal deposition parameter gave the best optical properties.

**Table 4.1: Sputter deposition parameters**

<i>Variables</i>	<i>Value used</i>
Pressure	$3.0 \times 10^{-3}$ , $6.0 \times 10^{-3}$ , $9.0 \times 10^{-3}$ (mbars)
Power	250W, 190W, 130W
Time of deposition	52 minutes
Substrate to target distance	65 mm
Gas flow rate	100 sccm

### 4.2. Thin film deposition

The plasma was excited by RF power supply working at a frequency of 13.6 MHz in a Dressler Caesar 136 sputtering system with RF matching network. The deposition was done using the Edwards Auto 306 sputtering coating unit. The Auto 306 was equipped with a turbo molecular pump which could achieve a pump down pressure of approximately  $3.2 \times 10^{-5}$  mbars within 60 – 90 minutes. The pressure inside the chamber was monitored using a Pirani gauge capable of monitoring atmospheric to a sub-atmospheric pressure. During the deposition, the thickness

of the sample was monitored by maintaining uniform sputtering time using a stop watch and the FTM6 thickness monitor on the coating unit.

Three different TiO<sub>2</sub> ceramic targets (High Purity Chemical Lab. Corp., Grade 99.99%) were used namely the pure Titanium dioxide, Titanium dioxide doped with niobium at 2% wt and Titanium dioxide doped with niobium at 4% wt. All three targets were of standard measurement of 100 mm in diameter and a thickness of 5 mm. Before sputtering could commence, the sputtering chamber was pumped down and evacuated to a base pressure of  $4.0 \times 10^{-5}$  mbars. Argon 99.995% was used as the sputter gas, was introduced at a constant flow rate of 100 cm/minute (standard cubic centimetre per minute). The sputter gas was being introduced into the chamber via the Alicat Scientific gas flow meter controller capable of varying the flow rate.

The working power and working pressure were modified during the deposition process. The gas flow rate and the substrate to target distance were kept constant. The deposition temperature was not altered by any external heating, but the high temperature in the chamber due to the plasma bombardment was between 120 °C and 140 °C.

A pre-deposition of 10 minutes was performed when starting to deposit using the new target and 5 minutes for subsequent samples as a method of cleaning exercise of the target and remove any impurities. After deposition, the unloading of the sample was only done after 10 minutes. This allowed cooling down of the chamber before venting to avoid any reactions of the film with air at those elevated temperatures.

### **4.3 Properties of the thin films**

Three properties of the deposited films were investigated, that is the optical, electrical and gas sensing properties.

#### ***4.3.1 Optical measurements of the thin film***

The optical spectral measurement was done in the UV-VIS-NIR region using the double beam solid spec Shimadzu™ model DUV 3700 Spectrophotometer. The spectral transmittance  $T(\lambda)$  and reflectance  $R(\lambda)$  for as-deposited and annealed samples were measured within the wavelength range of 300-2500 nm. The data for optical transmittance and reflectance at near incidence was collected and analysed to obtain bandgap energy using a well-known set of equations as discussed in section 3.2 (d).

#### ***4.3.1 Electrical properties measurements of the thin film***

The electrical measurements of the thin films were done using the Jandel RM3-AR four-point probe as shown and discussed in figure 3.3 c. the measurement was done by measuring the sheet resistance of the thin films, the values obtained were recorded directly without any further analysis. Measurement was done at different points to ensure anisotropy.

#### 4.4 Gas sensing properties measurement

The gas sensing properties were measured in a dome-shaped gas sensing unit set up as in the figure shown below.

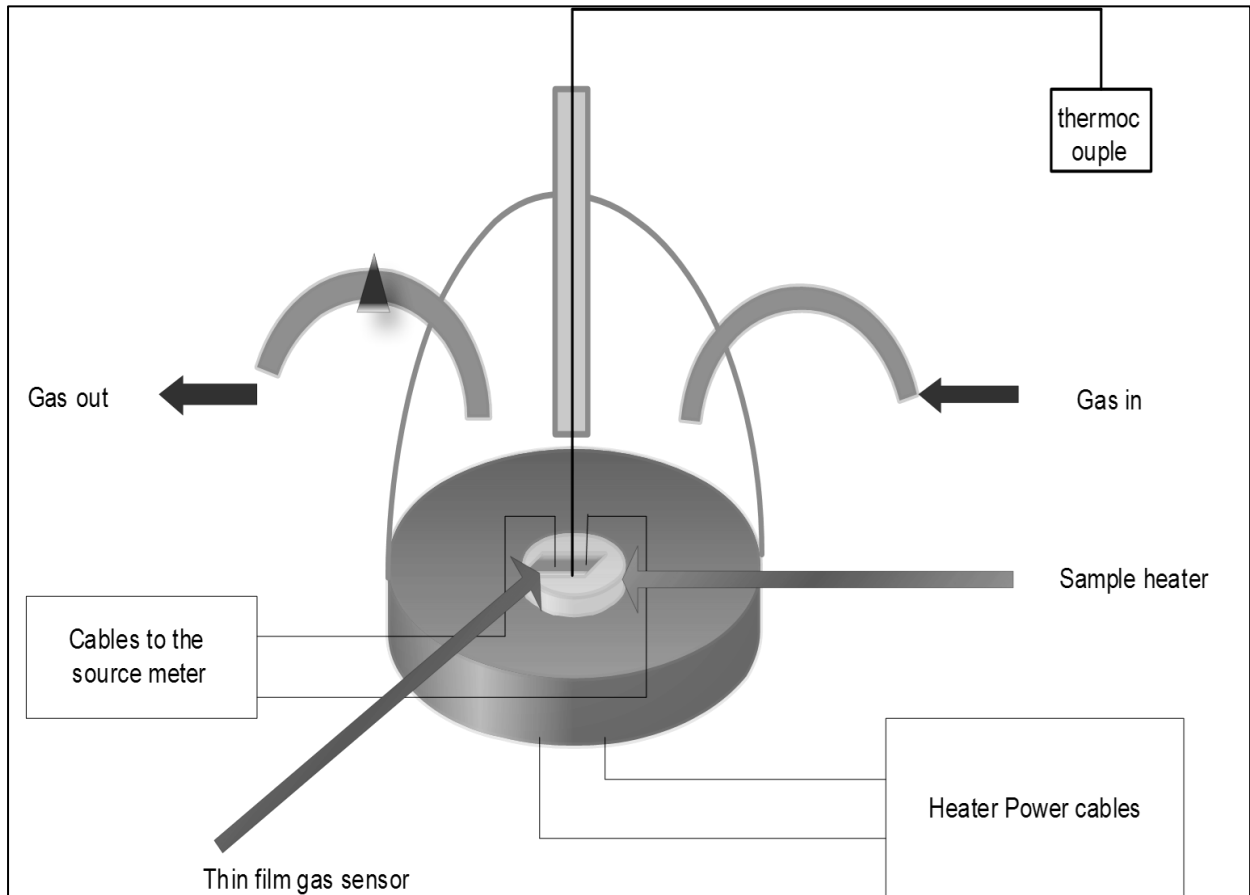


**Figure 4.1: The lab assembled gas sensing unit**

The Keithley 2400 source meter was used for resistance measurement of the samples. A heating resistor used in heating samples and the thermocouple were used to control the desired sample temperature. The temperatures of the samples were varied between 50°C and 300°C and resistance measurements in the air ( $R_a$ ), were taken at 25°C intervals.

A volume of gas (2000 ppm) as compared to the chamber volume (2.4 L) is to diffuse in the chamber for about 10 min at room temperature.

The sample temperature then was raised at a rate of 5°C/min and resistance measurements in a hydrogen environment ( $R_g$ ) for samples, were taken at 25°C intervals when there was hydrogen gas flow.

The electrical resistance when gas is flowing ( $R_g$ ), of the samples for each temperature intervals, was measured. The sample sensitivity ( $S$ ) for the gas of thin film was determined using the following equation;

$$S = \frac{R_a}{R_g} \dots\dots\dots 16$$

Where  $R_g$  is the sample resistance in test gas presence and  $R_a$  is the sample resistance in air.

## CHAPTER FIVE: RESULTS AND DISCUSSIONS

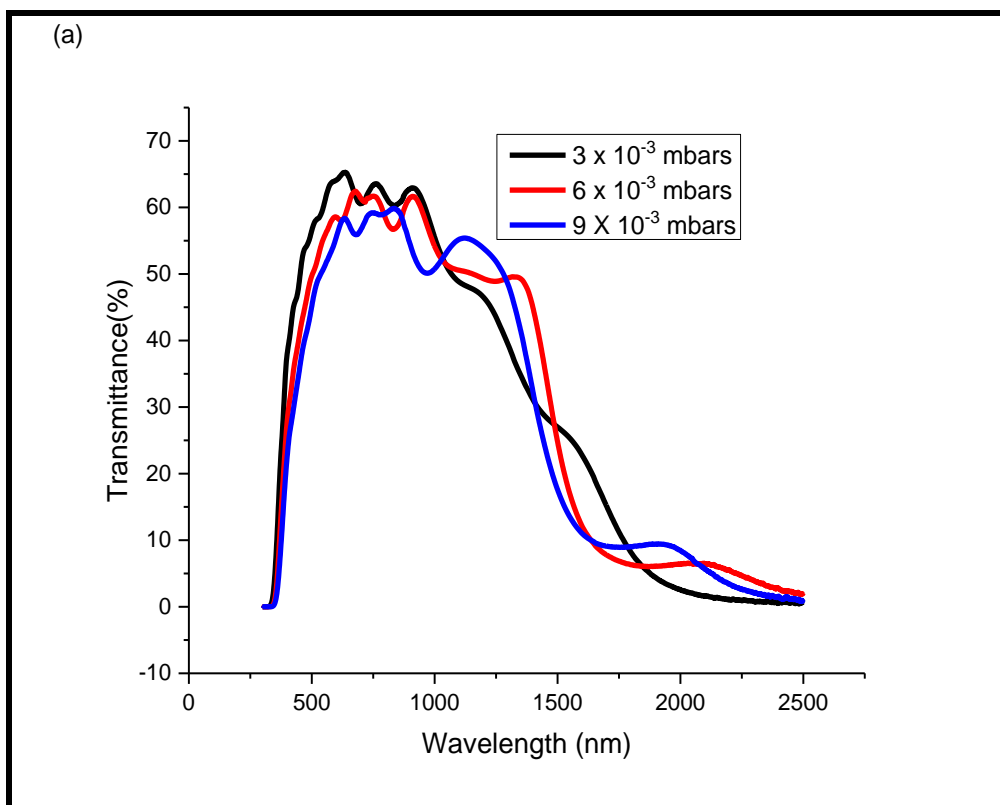
### 5.1 Introduction

Results based on optical and electrical properties for as-deposited and annealed samples for the undoped TiO<sub>2</sub> and Nb doped TiO<sub>2</sub> thin films were analysed and discussed in this chapter. To understand the effect of doping on the optical and electrical properties of TiO<sub>2</sub> thin films, results based on these properties for as-deposited and annealed samples are presented and compared under the various deposition conditions in this chapter. The gas sensing properties results for the pure and doped thin films are also discussed.

### 5.2 Optical properties of Nb doped TiO<sub>2</sub> thin films

#### 5.2.1 Influence of variations in deposition pressure on transmittance

The results presented below were collected using the UV probe software via a computer interfaced to a UV-VIS-NIR Spectrophotometer for experimental data for pristine TiO<sub>2</sub>, and niobium doped at 2 % wt TiO<sub>2</sub> and 4% wt TiO<sub>2</sub>, respectively. The data collected was uploaded to Microsoft Excel since it is versatile with built-in functions and the ability to make custom made functions using Excel VBA, with the data loaded, various calculations were now possible, thereafter the graphs shown in figure 5.1 a, b and c were plotted using Origin™ software which was preferred because of its fine rendering of graphs.



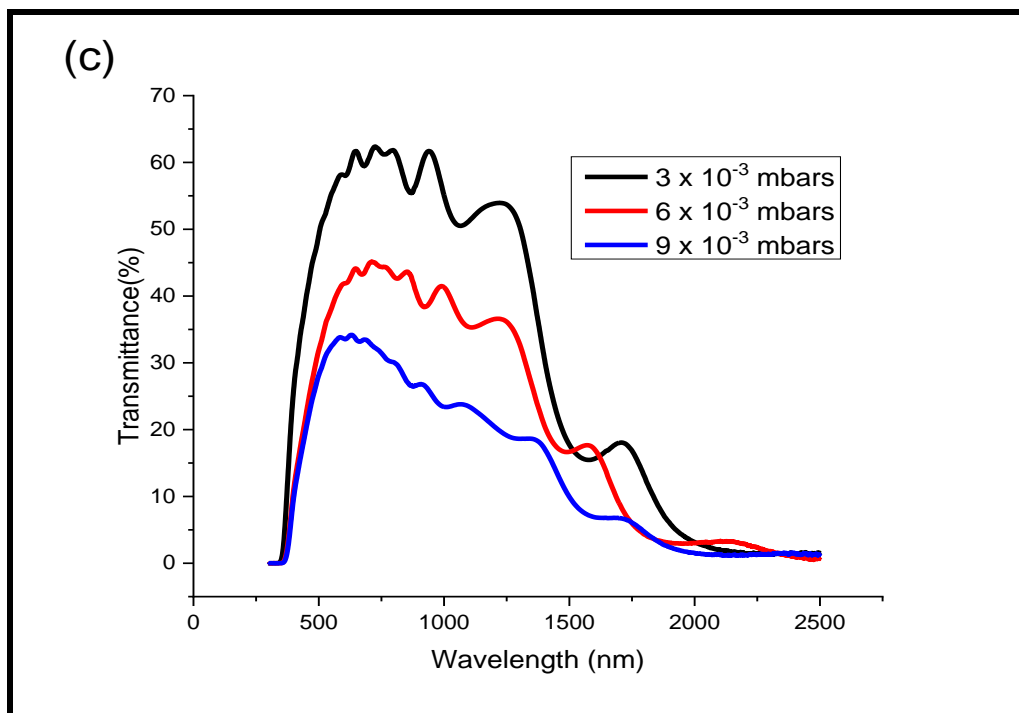
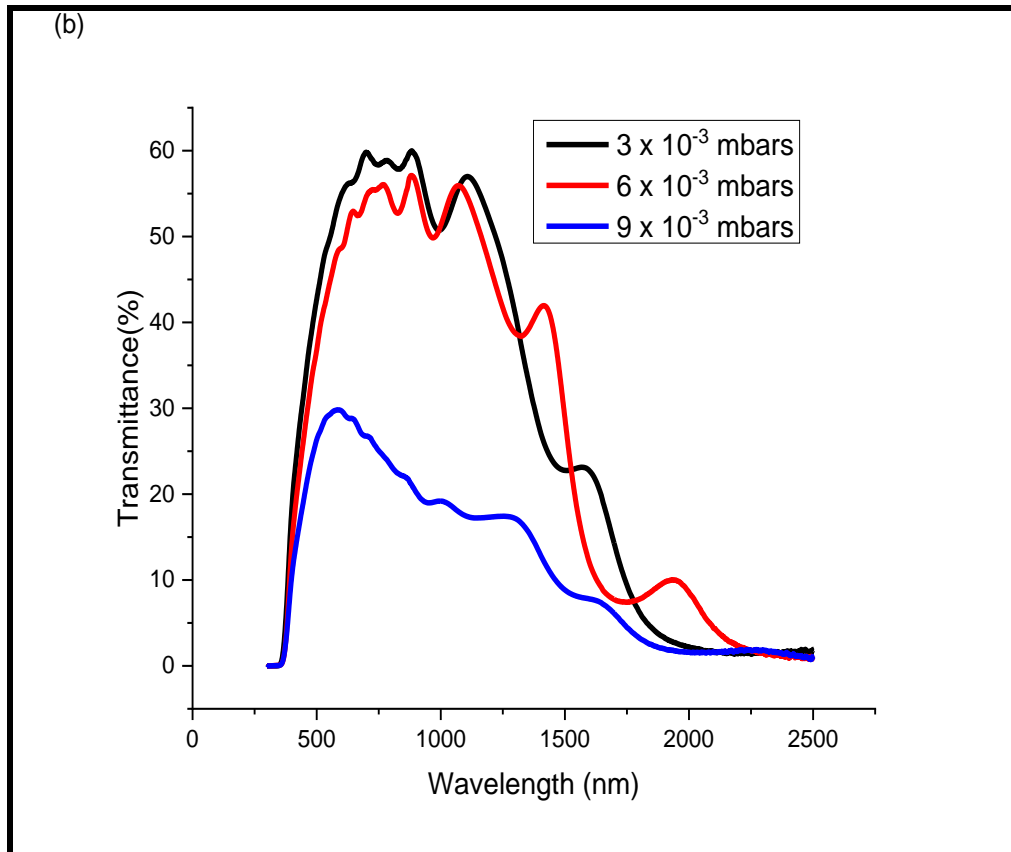


**Figure 5.1: Variations in the transmittance spectra for the TiO<sub>2</sub> thin films at different deposition pressure.**

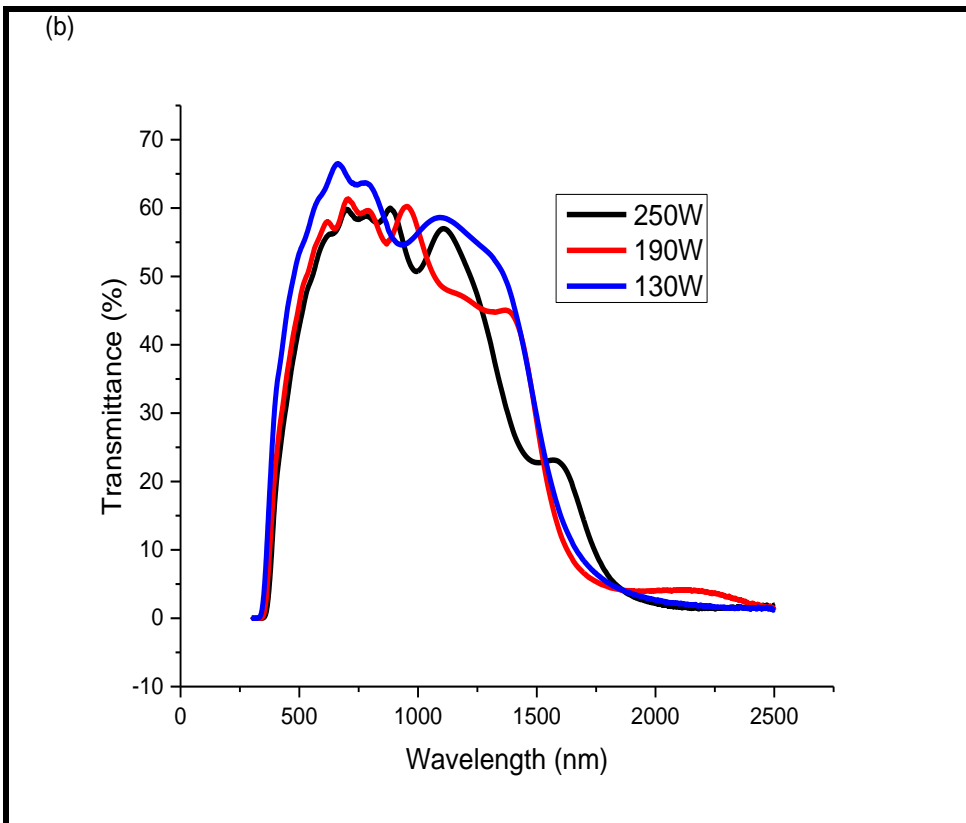
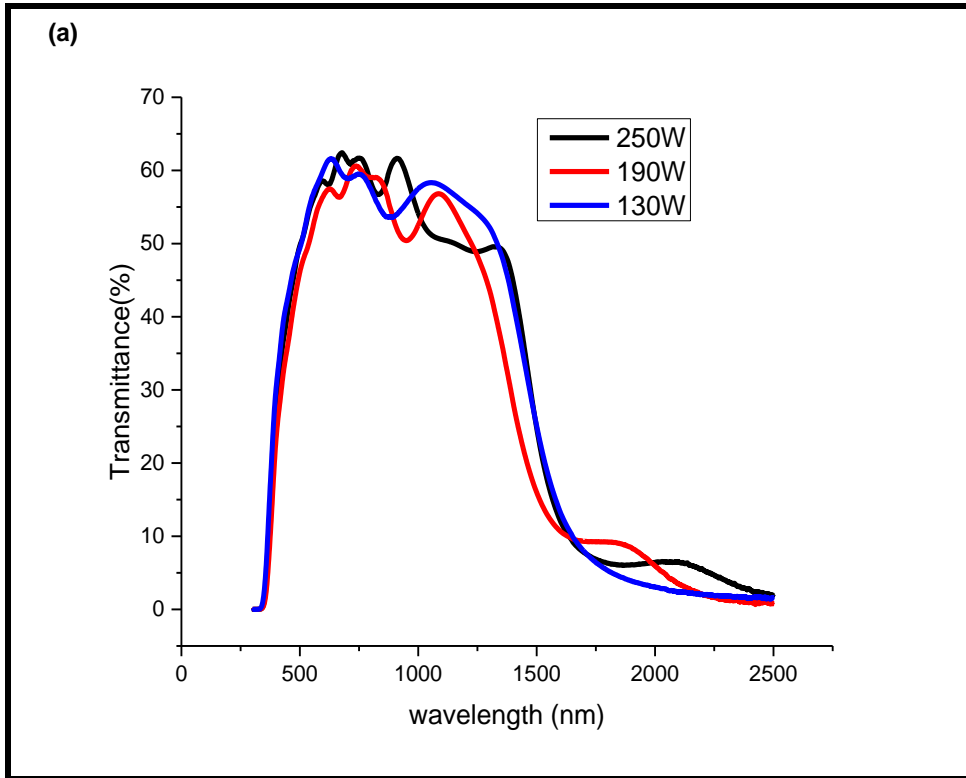
From figure 5.1 it is noted the highest transmittance was observed in the visible region for all the different material samples. However, it is also noted for the figure 4.1 that an increase in

the pressure led to a shift towards the visible range in the transmission edge which was a uniform finding for all the three materials. In figure 4.1 (a) is noted that for the pure TiO<sub>2</sub> samples there is just a slight decrease in transmittance when the deposition pressure is increased from  $3 \times 10^{-3}$  mbars, to  $6 \times 10^{-3}$  mbars and then to  $9 \times 10^{-3}$  mbars, in figure 5.1, the changes observed may be attributed to deficiency in oxygen due to the introduction of the sputter gas at different volume thereby changing the partial pressure (b) for the 2% Nb doped TiO<sub>2</sub> there is still a slight decrease in the transmittance when the deposition pressure is increased from of  $3 \times 10^{-3}$  mbars to  $6 \times 10^{-3}$  mbars and when the deposition pressure is further increased to  $9 \times 10^{-3}$  mbars there is a significant drop in the transmittance and for the 4% Nb-dopedTiO<sub>2</sub> there was a large significant drop in the transmittance as the deposition temperature is increased.

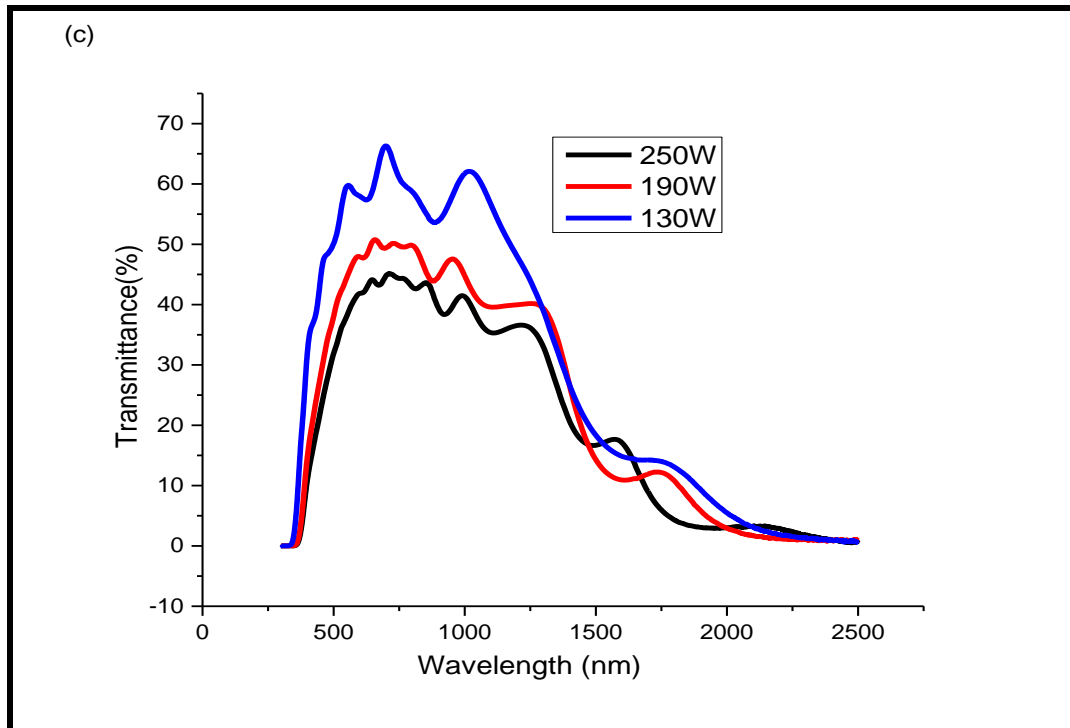
The above results imply that changes in the deposition pressure seem not to have any influence on the transmittance for the pure TiO<sub>2</sub> thin films whereas in the 2% doped TiO<sub>2</sub> thin film changes in pressures lower than  $6 \times 10^{-3}$  mbars have no significant change in transmittance and pressures higher than the above pressure seem to have a strong influence on the transmittance obtained. In the 4 % Nb doped TiO<sub>2</sub>, any change in the deposition pressure is bound to have a significant influence on the transmittance, the change observed is attributed to oxygen competition between Niobium and TiO<sub>2</sub>.

### **5.2.2. Influence of variations in deposition power in transmittance**

To determine the effect of deposition power on the thin films prepared the deposition was varied as follows 130 W, 190 W and 250W.



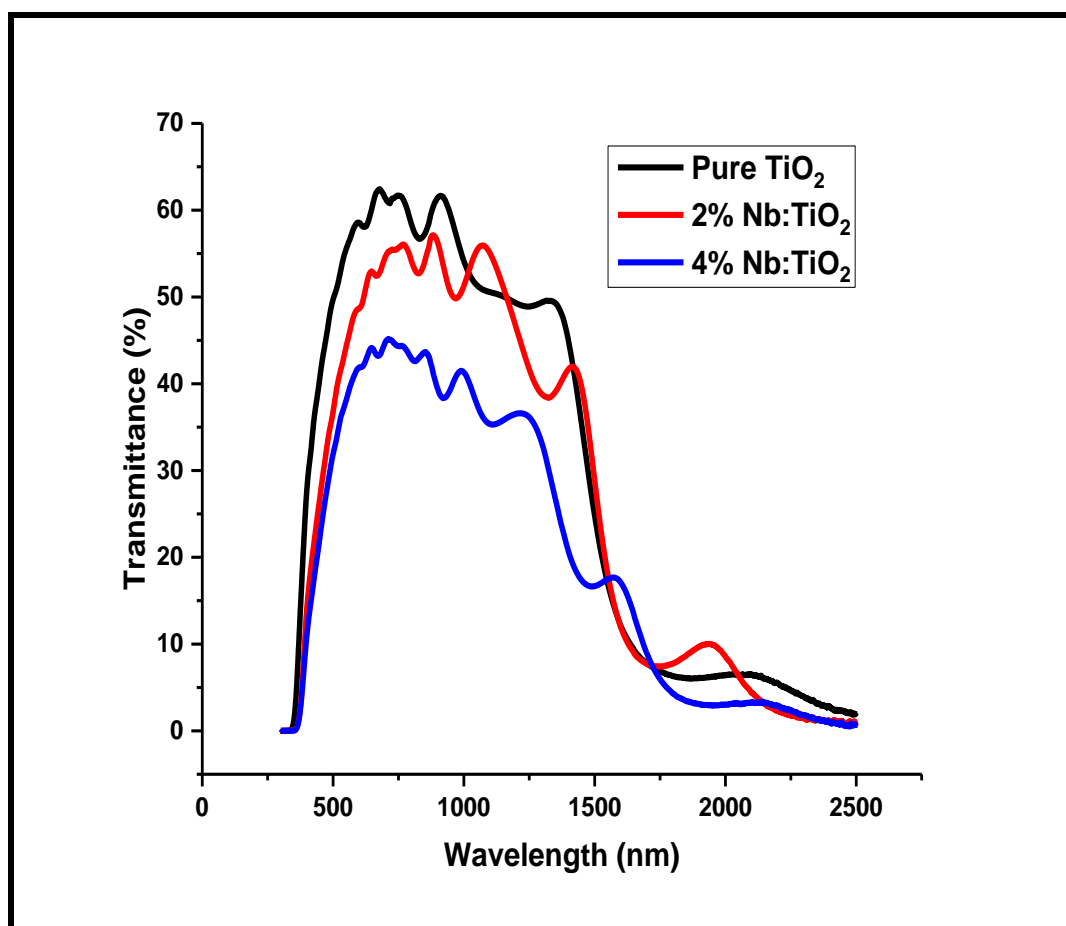




**Figure 5.2: The transmittance spectra for the thin films deposited at various RF power.**

From figure 5.2(a), it's seen that for the pure  $\text{TiO}_2$  samples when the power is decreased from 250W to 190W and then to 130W there is just a slight change in transmittance this change is not significant enough to have any impact on the transmittance, in the 2% Nb doped  $\text{TiO}_2$  samples, figure 5.2(b), it's noted that the same trend as in the pure  $\text{TiO}_2$  samples is seen though now it is noted that lower deposition power gives us the highest transmittance and finally in the 4% Nb doped  $\text{TiO}_2$  samples, figure 5.2(c) it is noted that increasing the deposition power leads to a tremendous drop in the transmittance. This implies that increasing the deposition power has no significant effect on transmittance for the pure  $\text{TiO}_2$  thin films whereas in the 2% Nb doped  $\text{TiO}_2$  samples there is a slight drop in the transmittance as the deposition power is increased though it's seen that at powers higher than 190W there is no significant change in the transmittance, and in the 4% Nb doped  $\text{TiO}_2$  films an increase in the deposition power results into a decrease in the transmittance. The deposition power influences the growth of the thin film, high transmittance implies that a thinner film was formed while with the increase in power a thicker film was formed, therefore the transmittance is in agreement with Lambert-Beers law of transmittance.

### 5.2.3. Influence of niobium doping on transmittance



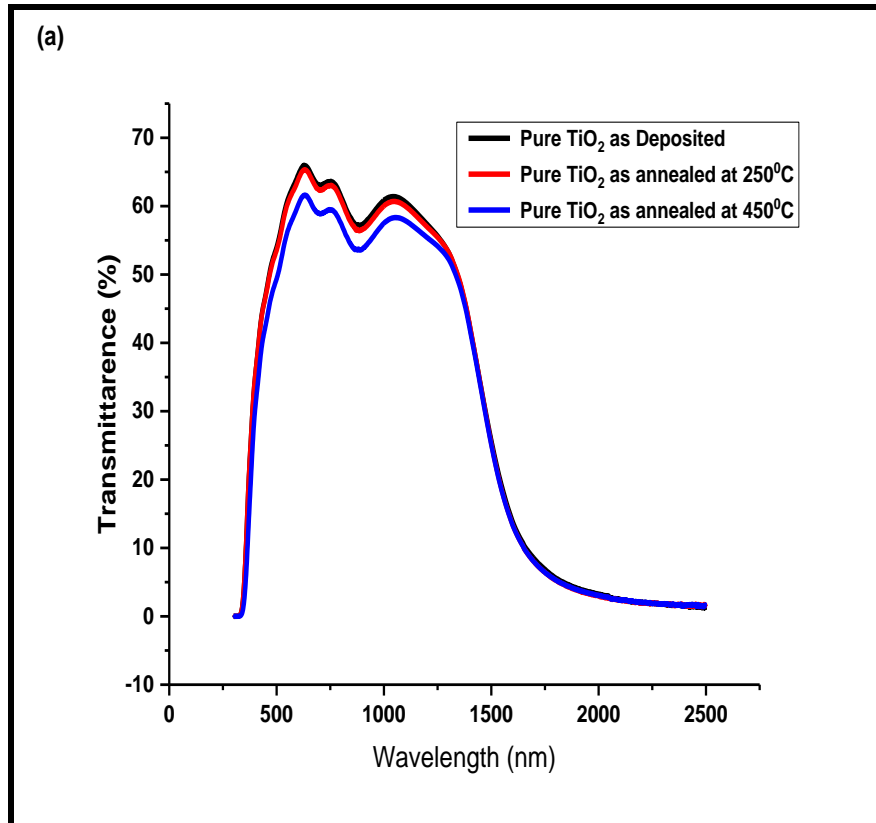
**Figure 5.3: The transmittance spectra for pure and Nb-doped TiO<sub>2</sub> thin films deposited.**

Figure 5.3 above is the measured transmission spectra obtained when the pure and the Nb-doped TiO<sub>2</sub> are deposited in same RF power of 250W and same sputtering pressure of  $6 \times 10^{-3}$  mbars. It is seen that doping of the TiO<sub>2</sub> causes a reduction in the transmittance in visible and up to the near infra-red. 4% Nb-doped TiO<sub>2</sub> gives the lowest transmittance for this sputtering condition and therefore a reduction in transmittance was depended on the amount dopant in the material. This reduction can be attributed to the increase in free electrons and change of band gap of the composite material, this observation is in good agreement with Drude's theory as corroborated by the work done by Sato *et al.*, (2010).

### 5.2.4. Influence of annealing on optical transmittance

The figure 5.4 below shows the transmittance spectra for the as-deposited and as post annealed at 250°C and 450 °C. The samples were deposited on the same deposition conditions, that is, 130W RF power and  $6.0 \times 10^{-3}$  mbars, where figure 5.4 (a, b and c) are the transmittances for pure, 2% Nb-doped and 4% Nb-doped samples. From the graphs, it can be shown that for these

annealing temperatures, there was only a slight decrease in transmittance for all the samples of the undoped and Nb doped TiO<sub>2</sub> samples. This slight decrease in transmittance can be attributed to increased light scattering effect due to increased surface roughness (Hasan *et al.*, (2008).



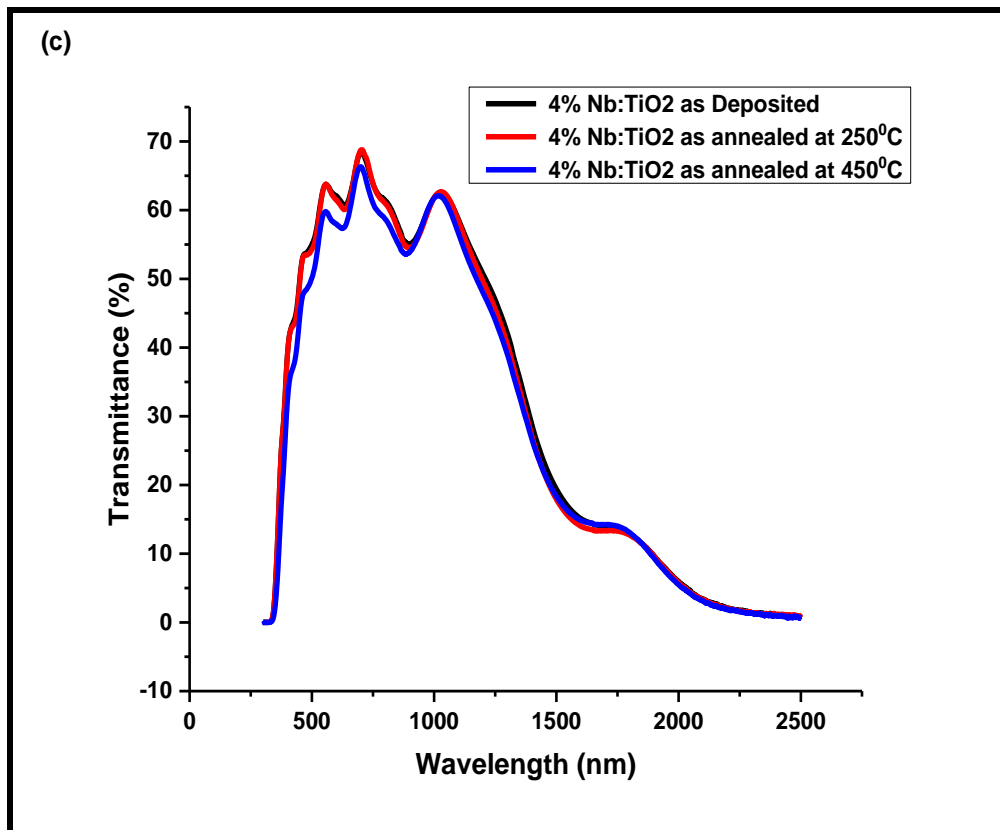
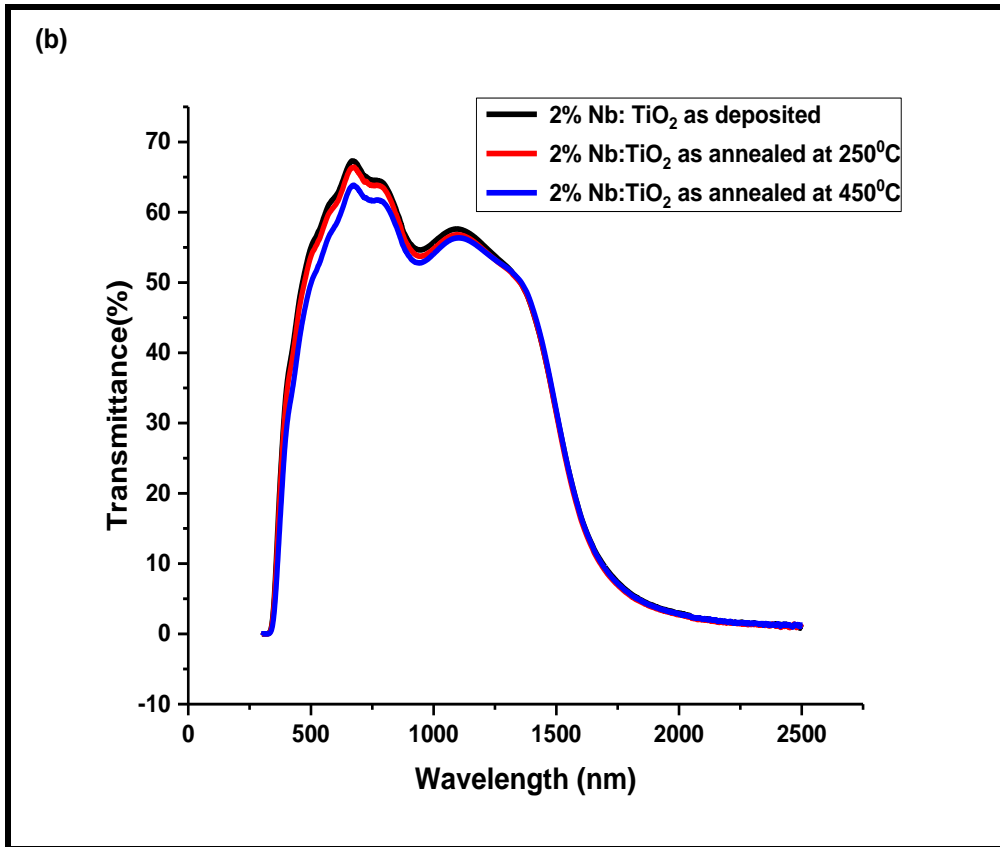
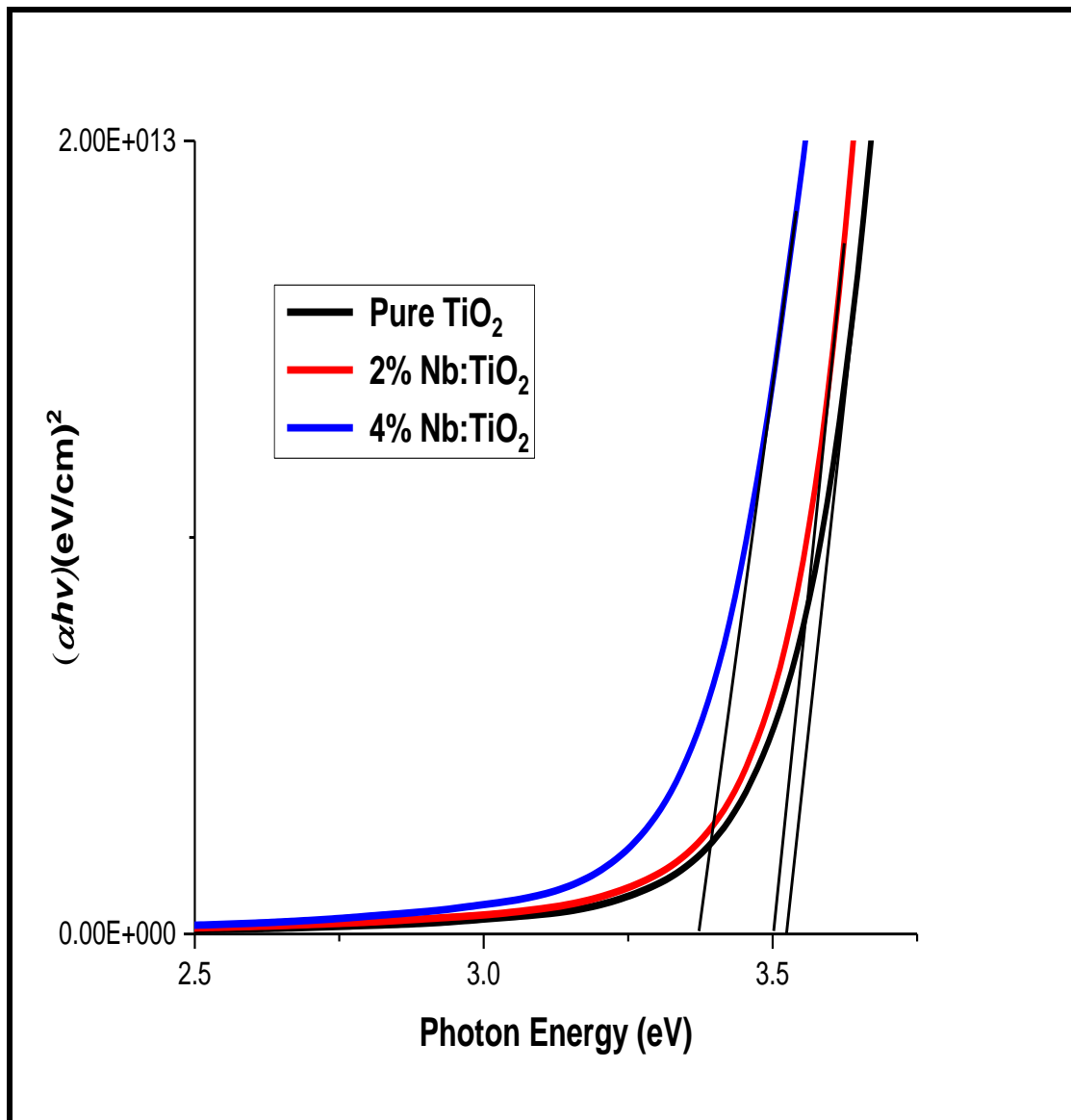


Figure 5.4: The transmittance spectra for the thin films as-deposited and annealed

### 5.3. Optical band gap of the thin films

The band gaps ( $E_g$ ) were obtained from the extrapolation's method for the deposited samples, based on the assumption of directly allowed transitions to an empty conduction band for the suspected dominant anatase  $\text{TiO}_2$ .

#### 5.3.1 Optical band gap for as-deposited thin films



**Figure 5.5: The Band gap curves for as-deposited thin films as deposited**

From figure 5.5 above it was established that the band gap reduced with an increase in the level of doping. As indicated by the tangents of the linear parts of the curves, the band gaps obtained reduced from 3.53eV to 3.50eV and then to 3.37eV for pure, 2% and 4% Nb-doped  $\text{TiO}_2$  thin films, respectively. This implies that increase in Nb doping content leads to a decrease in band

gap which can be attributed to the shift in the absorption edge band gap towards the visible range of the films as seen in the transmittance plot in section 5.2.3(Uyanga *et al.*, (2014).

### 5.3.2. Optical band gaps for the post annealed (450°C) for the thin films

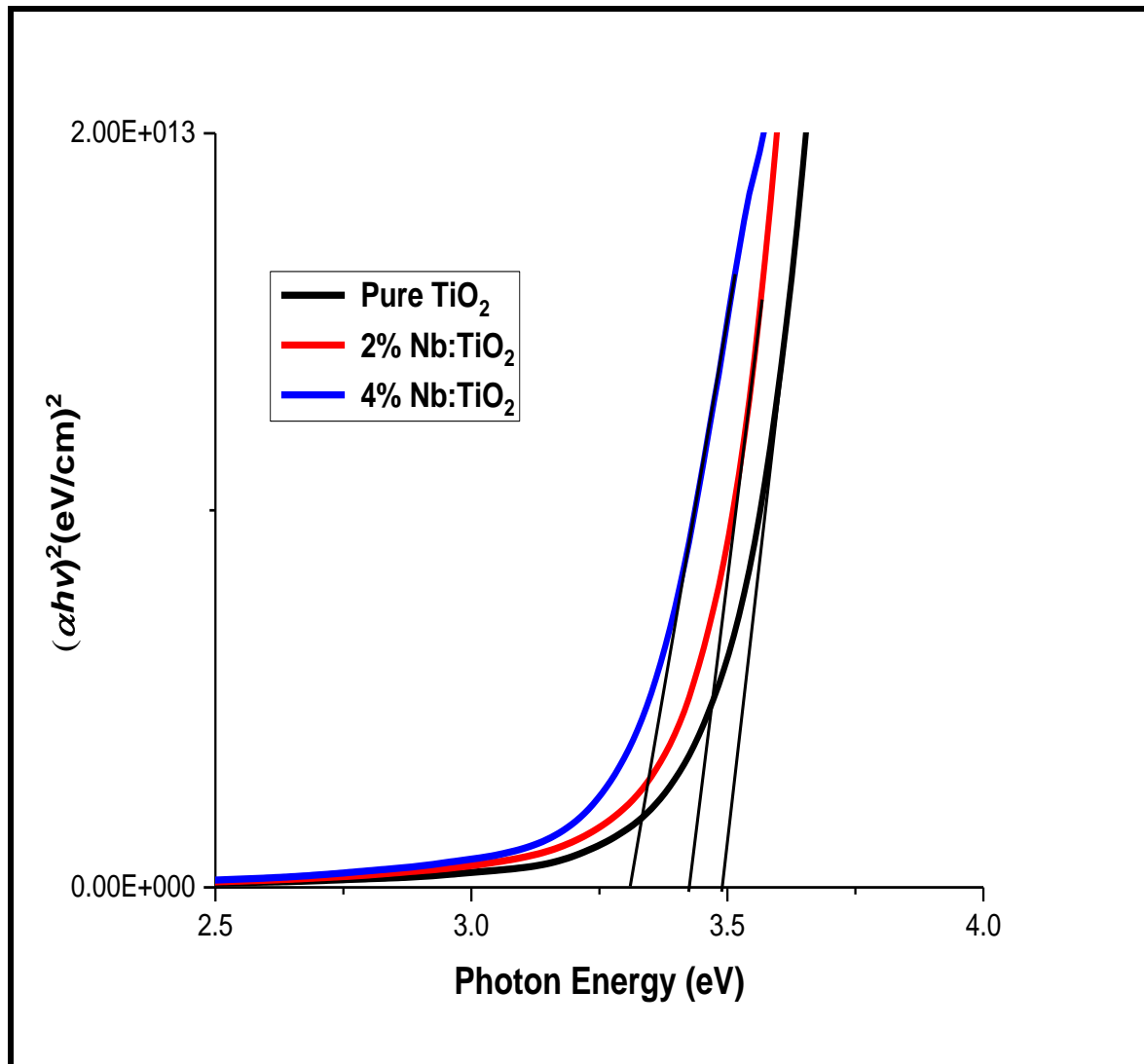


**Figure 5.6: Band gap curves for the post annealed films**

The band gaps obtained after annealing (figure 5.6) indicates a drop in band gap for the pure and the doped samples. The results can be summarized as in table 5.1 below.

**Table 5.1: Comparison of band gaps as annealed and as-deposited**

Sample	Band gap as-deposited	Post annealed band gap
Pure TiO <sub>2</sub>	3.53	3.49
2% Nb- doped TiO <sub>2</sub>	3.50	3.42
4% Nb- doped TiO <sub>2</sub>	3.37	3.31

The observed drop in the band gap of the materials before and after annealing may be attributed to change of structure from amorphous to crystalline structure. The variations in band gap observed are indications of structural modifications. The structural modification is caused by some of the prevailing deposition conditions and post-deposition conditions as annealing (Kil D., 2005). This shift in the optical band gap to lower values after annealing may be related to a change in film density and an increase in grain size as also reported by other researchers (Van-son *et al.*, 2014).

#### 5.4. Electrical properties of pure and doped TiO<sub>2</sub> thin films

The measured sheet resistance used to determine electrical resistivity and conductance for the as-deposited and annealed thin films. Similarly, results for the bulk resistivity are presented.

The sheet and bulk resistivity were done using the Jandel RM3-AR four-point probe. The electrical conductivity  $\rho$  was determined using the formula (Ayodele *et al.*, 2014).

$$\rho = R_s \times t \dots\dots\dots 17$$

The measured sheet resistance and the calculated electrical resistivity and conductivity (inverse of resistivity) were tabulated in table 5.2 below. From the table, it can be realized that the doping of TiO<sub>2</sub> thin films increases its conductivity. The increased conductivity can be attributed to the increased number of carrier concentration.

##### 5.4.1. Electrical properties of the thin films as-deposited

**Table 5.2: Summary of the electrical properties as- deposited**

Parameters	PureTiO <sub>2</sub>	2% Nb:TiO <sub>2</sub>	4%Nb:TiO <sub>2</sub>
Sheet Resistance, R <sub>s</sub> (Ω/Sq.)	4393.03	617.2494	0.59374
Electrical resistivity, ρ (Ω.cm)	2.2844X10 <sup>-2</sup>	3.2097X10 <sup>-3</sup>	3.0874X10 <sup>-6</sup>
Electrical conductivity,σ (Ω <sup>-1</sup> cm <sup>-1</sup> )	4.3776X10 <sup>1</sup>	3.1156X10 <sup>2</sup>	3.2389x10 <sup>5</sup>

Table 5.2 showed that the resistivity decreased as the level of doping increased. The reduction in resistivity can be attributed to an increase in carrier density when doping is increased. The resulting rise in carrier density is because of the increasing amount of electrically activated charge carriers. The same trend is observed when the samples were post annealed at a temperature of 450 °C as shown in table 5.4 below.

#### 5.4.2. Electrical properties of pure and TiO<sub>2</sub> thin films as annealed

**Table 5.4: Summary of electrical properties for samples annealed at 450 °C**

Parameters	Pure TiO <sub>2</sub>	2%Nb:TiO <sub>2</sub>	4%Nb:TiO <sub>2</sub>
Sheet resistance $R_s$ ( $\Omega$ /sq)	4111.940	0.122375	0.04759
Electrical resistivity ( $\Omega$ .cm)	$2.1383 \times 10^{-2}$	$6.3635 \times 10^{-7}$	$2.4747 \times 10^{-13}$
Electrical conductivity ( $\Omega^{-1}$ .cm <sup>-1</sup> )	$4.6768 \times 10^1$	$1.5715 \times 10^6$	$4.0409 \times 10^{12}$

#### 5.4.3. Comparison of electrical resistivity of the films as deposited and as annealed

**Table 5.5: The summary of the sheet resistance for the as-deposited and as annealed**

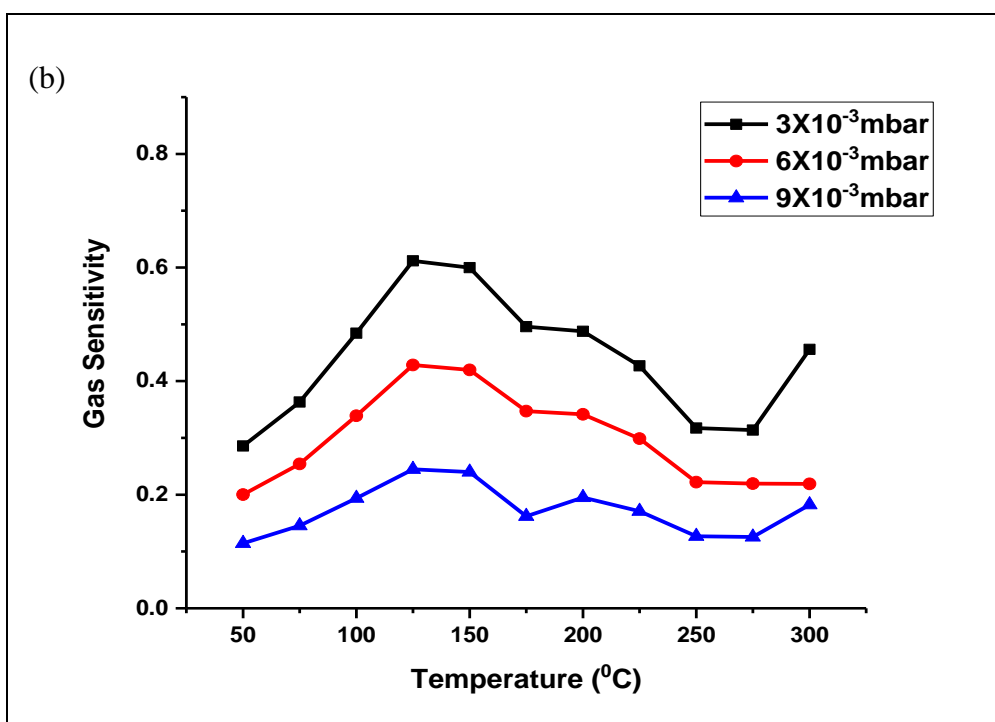
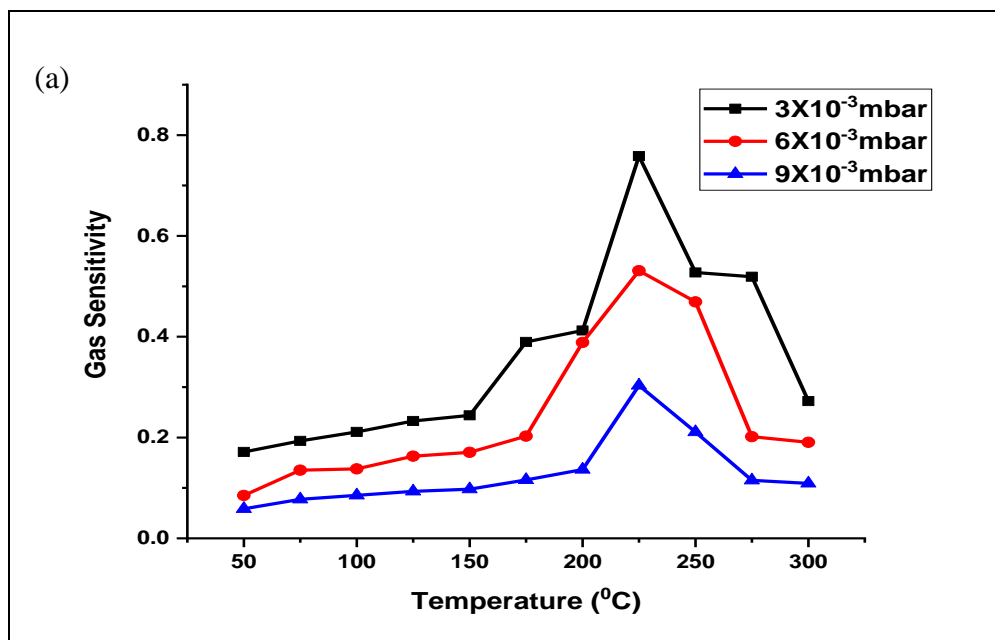
Sample	Sheet resistance as-deposited $\Omega$ /Sq.	Sheet resistivity annealed(450 °C) $\Omega$ /Sq.
PureTiO <sub>2</sub>	4393.03	4111.94
2% Nb:TiO <sub>2</sub>	617.2494	0.122375
4% Nb:TiO <sub>2</sub>	0.59374	0.04759

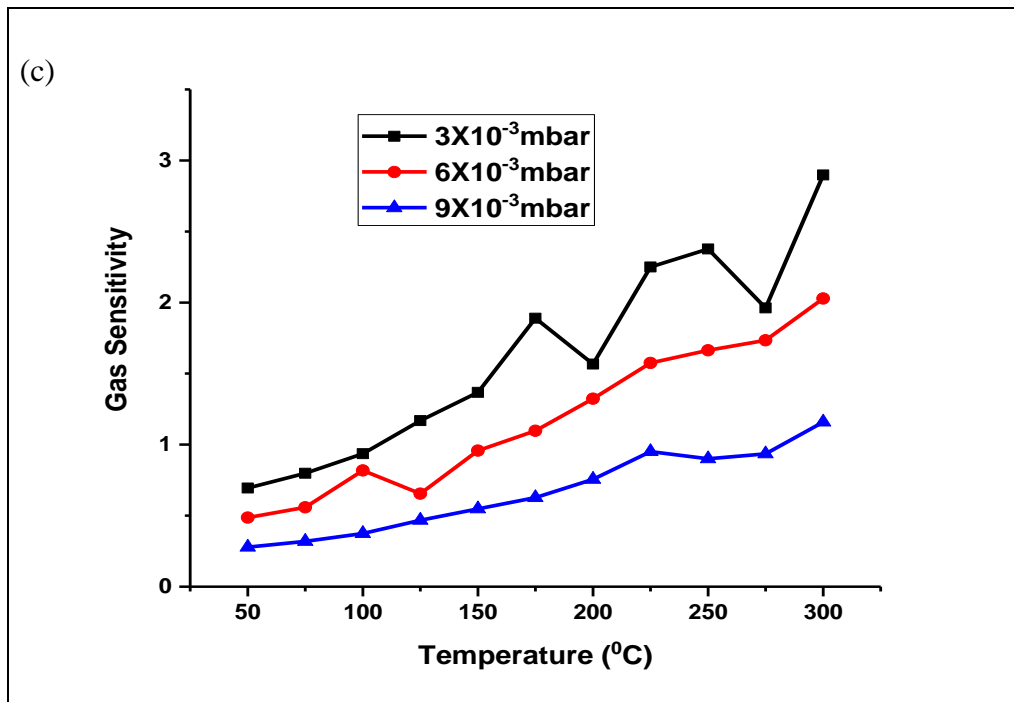
Table 5.5 shows that annealing led to a decrease in the sheet resistance for the pure TiO<sub>2</sub>, 2% Nb doped TiO<sub>2</sub> and 4% Nb doped TiO<sub>2</sub> samples. This implies that annealing improved the electrical conductivity of thin films.



## 5.5 Gas sensing properties

### 5.5.1 Influence of deposition pressure on the gas sensing properties

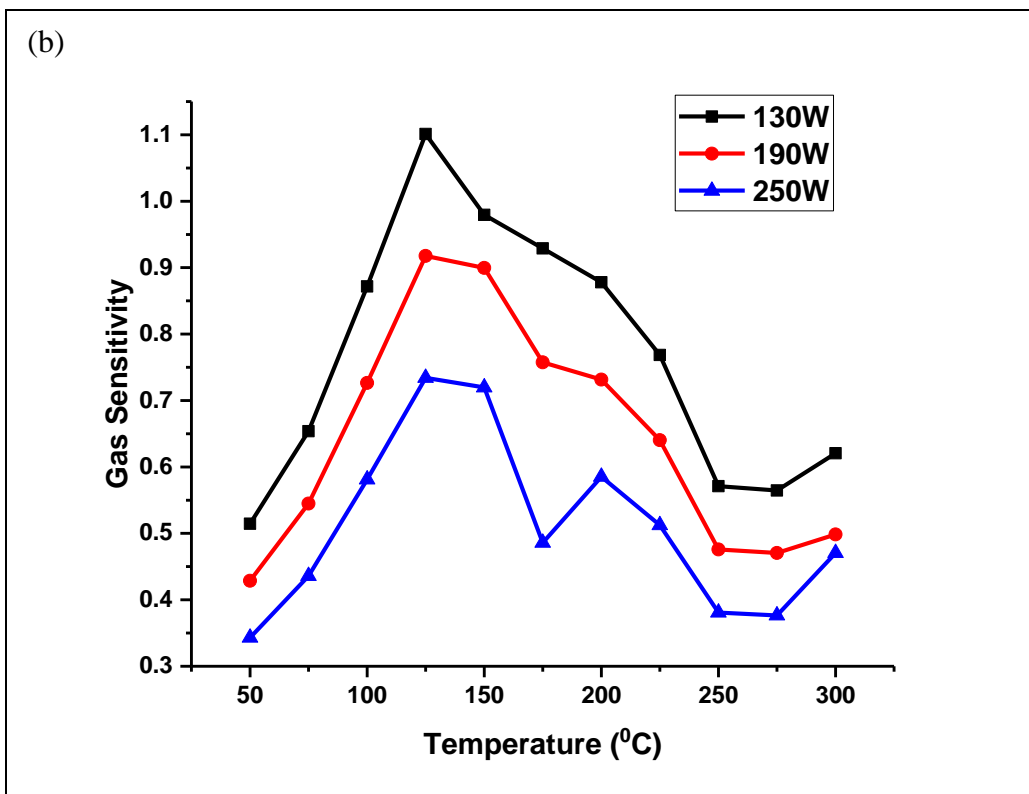
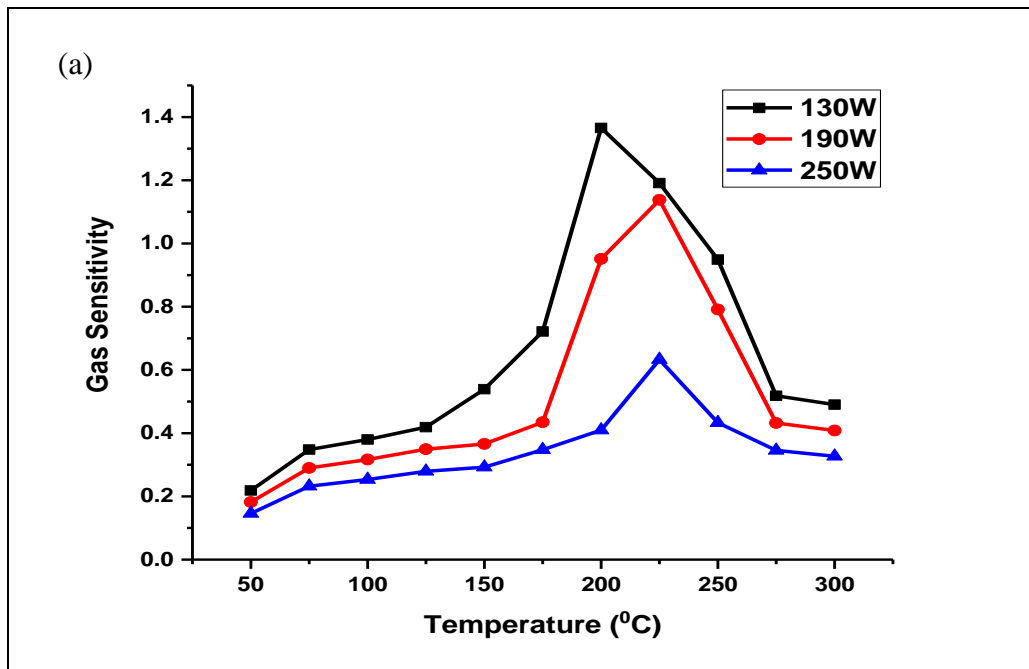


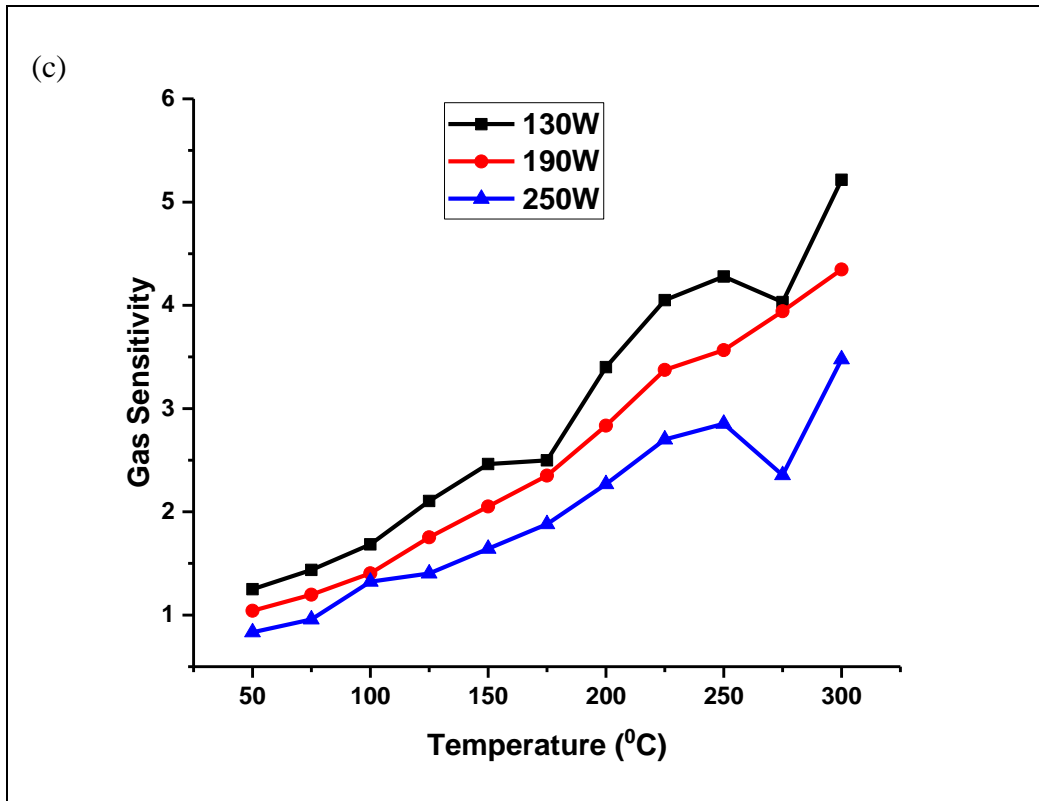


**Figure 5.6 Influence of deposition pressure on the gas sensing properties (a) undoped TiO<sub>2</sub>, (b) 2% Nb doped TiO<sub>2</sub> and (c) 4% Nb doped TiO<sub>2</sub>**

In figure 5.6 a,b,c its noted that as deposition pressure was increased there was a decrease in the gas sensing properties of the thin films for three types of materials, it is also observed that the thin films showed different gas sensitivity at different temperatures with the pure TiO<sub>2</sub> thin films showing a gas sensitivity temperature between 200 and 250<sup>0</sup>C, the 2 % Nb doped TiO<sub>2</sub> thin films in the 100- 150 <sup>0</sup>C temperature range and the 4% Nb doped TiO<sub>2</sub> thin films in the temperature range between 200-300<sup>0</sup>C. The 4% Nb doped TiO<sub>2</sub> thin film samples exhibited the highest gas sensitivity values which were between 0.5 and 3 (figure 5.6(c)). The 2% Nb doped TiO<sub>2</sub> and Undoped TiO<sub>2</sub> thin films had gas sensitivity values between 0.1 and 1 (figure 5.6 (a and b)).

5.5.2 Influence of Deposition power on the gas sensing properties

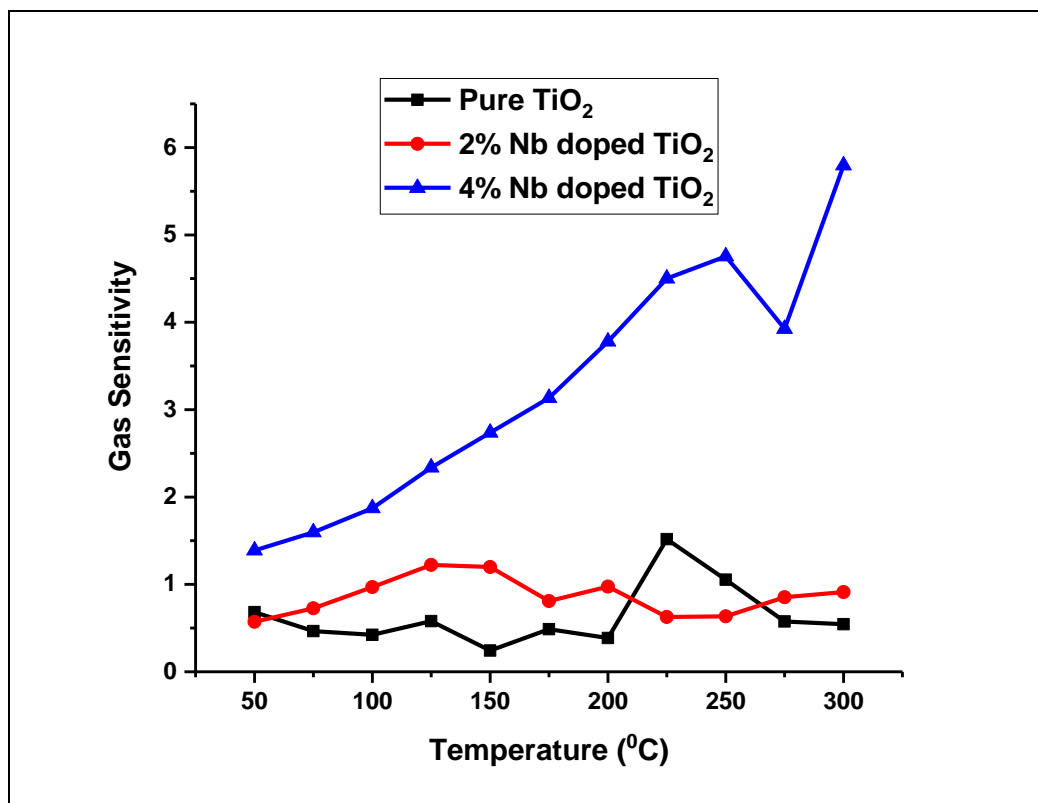




**Figure 5.7 Influence of deposition power on the gas sensing properties, (a) undoped TiO<sub>2</sub>, (b) 2%Nb doped TiO<sub>2</sub> and (c) 4% Nb doped TiO<sub>2</sub>**

From figure 5.7 when the deposition power was increased there was a decrease in the gas sensing properties of the thin films for three types of materials. It may be noted that the thin films showed different gas sensitivity temperatures with the pure TiO<sub>2</sub> thin films showing a gas sensitivity temperature between 200 and 250°C, the 2 % Nb doped TiO<sub>2</sub> thin films in the 100-150°C temperature range and the 4% Nb doped TiO<sub>2</sub> thin films in the temperature range between 200-300°C which correspond to those noted by during in the section 5, 5.1 above. The 4% Nb doped TiO<sub>2</sub> thin film samples exhibited the highest gas sensitivity values which were between 0.5 and 5.5 (figure 5.7(c)). The 2% Nb doped TiO<sub>2</sub> had gas sensitivity values between 0.2 and 1.1 (figure 5.7(b)) and the Undoped TiO<sub>2</sub> thin films had gas sensitivity values between 0.1 and 1.5 (figure 5.7(a)). this implies that the 4% Nb TiO<sub>2</sub> thin films showed a better gas sensitivity compared to the rest of the materials.

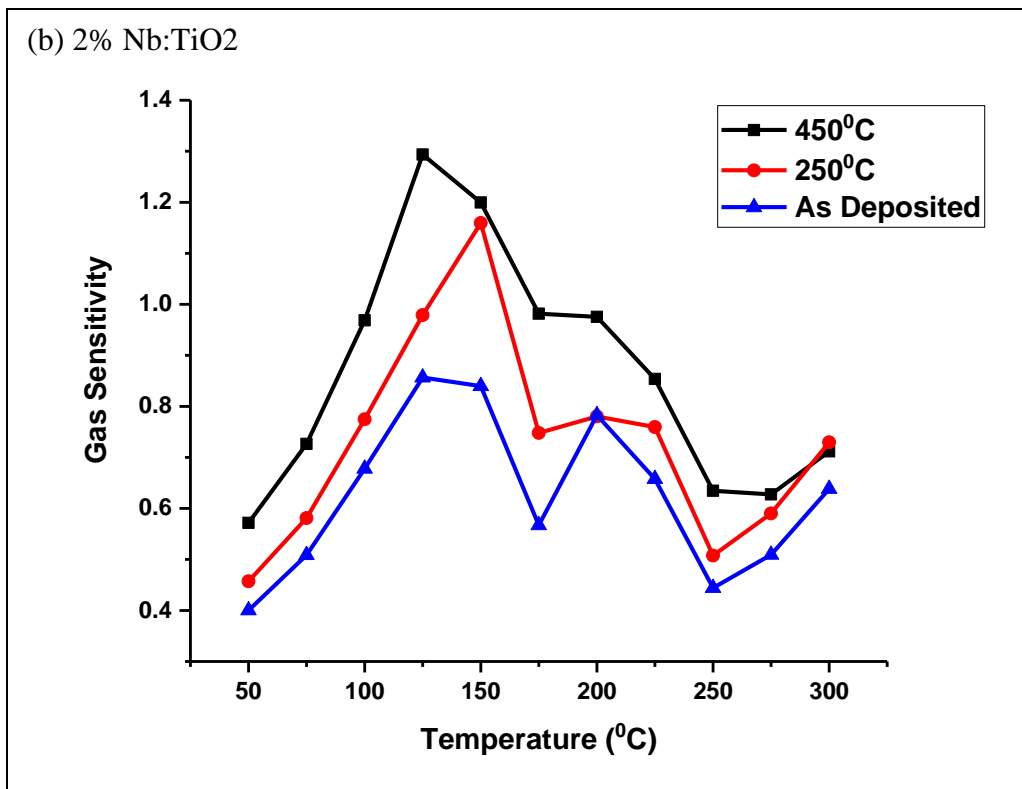
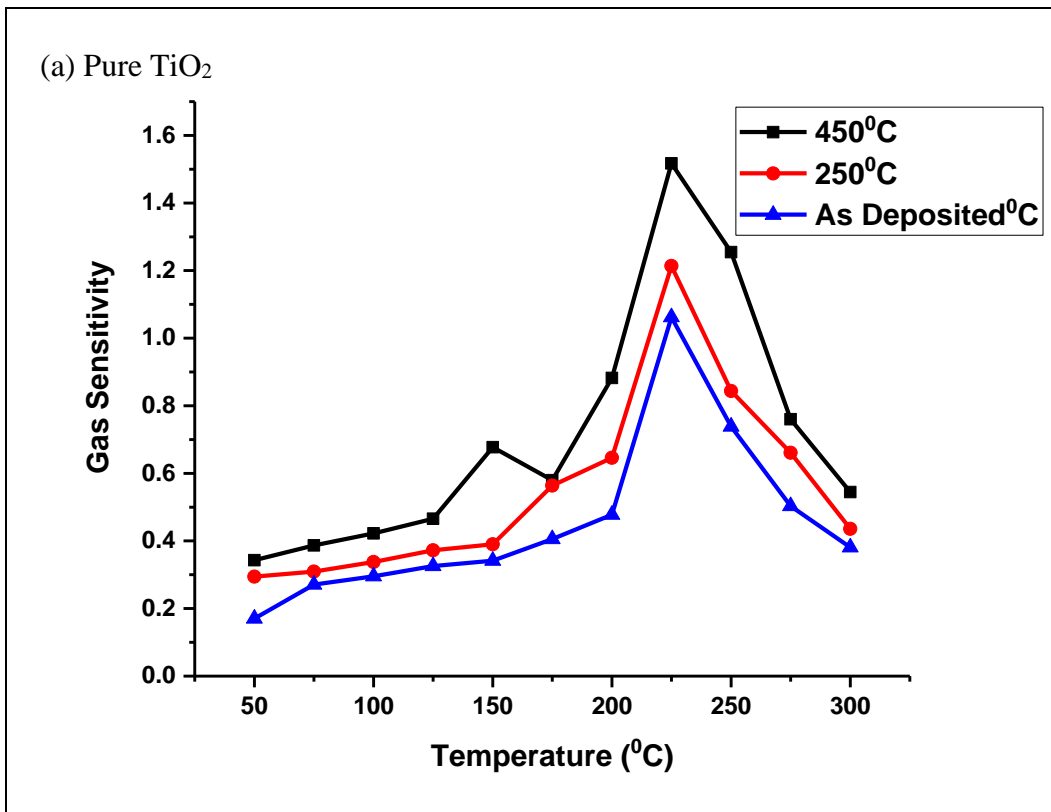
### 5.5.3 Influence of Niobium doping on the gas sensing properties of TiO<sub>2</sub> thin films



**Figure 5.8: Influence of Nb doping of TiO<sub>2</sub> on the gas sensing properties**

Figure 5.8 shows gas sensitivity versus temperature from the figure it is noted that 4% doped TiO<sub>2</sub> had the best gas sensing properties since the gas sensitivity ratio of this sample had increasing sensitivity with an increase in temperature. The pure TiO<sub>2</sub> films showed the worst gas sensitivity ratio in the temperature range 50<sup>0</sup>C to 200<sup>0</sup>C after this point the pure film showed better than the 2% Nb doped TiO<sub>2</sub> gas sensitivity until 250<sup>0</sup>C. The gas sensitivity temperatures for the three material were between 200-250<sup>0</sup>C, 100-175<sup>0</sup>C and 200- 300<sup>0</sup>C for the undoped TiO<sub>2</sub>, 2% Nb doped TiO<sub>2</sub> and 4% Nb doped TiO<sub>2</sub> thin films, respectively.

5.5.4 Influence of annealing temperatures on the gas sensing properties



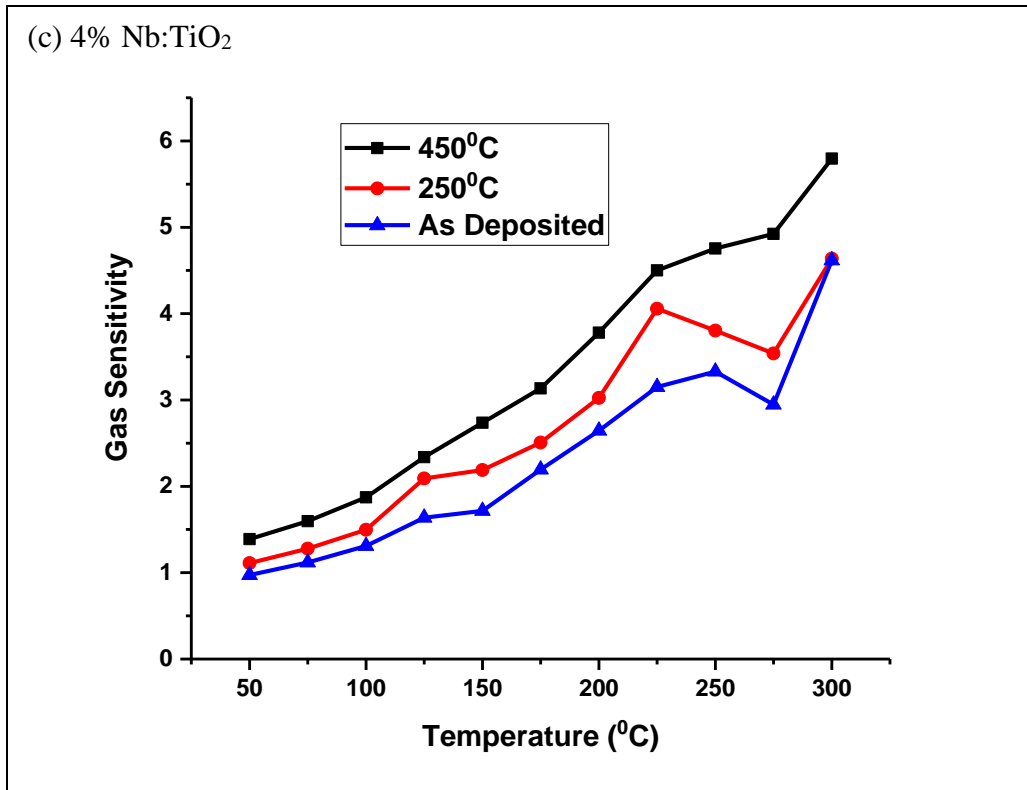


**Figure 5.9: Influence of annealing temperatures on the gas sensing properties,**

When the thin films were annealed it was noted that the samples annealed at 450°C produced the best gas sensing values in all the three materials this can be attributed to the increased crystalline phase the TiO<sub>2</sub> since at 450°C which is the rutile phase of the TiO<sub>2</sub>. In figure 5.9(a,b,c) its noted that there is a rise in the gas sensitivity of samples annealed at 450°C for the three materials while for the as-deposited and sample annealed at 250°C there is just a slight increase in the gas sensitivity values with the as-deposited sample having lower values.

## CHAPTER 6: CONCLUSION AND RECOMMENDATIONS

---

### 6.1 Conclusion

Nb doped TiO<sub>2</sub> and undoped TiO<sub>2</sub> films have been deposited by RF magnetron sputtering. The deposition of the films was done using the Edwards AUTO 306 vacuum system. The substrate used was Fluorine doped SnO (FTO) glass and before deposition, the FTO glass was cleaned ultrasonically using the Power-Sonic 405. The sputter targets used, were 3 with the composition ratios of Nb: TiO<sub>2</sub> being 2:98 wt% and 4:96 wt% with a purity of 99.99% and a 100% wt TiO<sub>2</sub> with 99.99% purity.

The thin films prepared were then analysed for their optical, electrical and gas sensing properties using the Shimadzu DUV 3700 series double beam spectrophotometer, Jandel RM3-AR four-point probe and gas sensing apparatus, respectively.

The optical results revealed that an increase in the sputtering pressure had no significant impact on the transmittance of the pure TiO<sub>2</sub> films. Whereas with the 2% Nb doped TiO<sub>2</sub> films there was no significant change in transmittance when the sputtering pressure was increased from  $3 \times 10^{-3}$  mbar to  $6 \times 10^{-3}$  mbars, however, when the sputtering pressure was increased further to  $9 \times 10^{-3}$  mbar it was noted that there was a significant drop in the transmittance this is because sputter pressure influences the uniformity of the resultant film with low pressures producing a uniform and single-crystal structure thin films. For the 4% Nb doped TiO<sub>2</sub> films it was noted that any increase in the sputtering pressure had a significant drop in transmittance.

The results further showed that a decrease in the sputter power had no significant drop in the transmittance for the pure TiO<sub>2</sub> and 2% Nb doped TiO<sub>2</sub> films. When it came to the 4% doped TiO<sub>2</sub> films it was noted that a decrease in the sputter power had a significant decrease in the transmittance. The average transmittance was 60%, 45% and 40% for sputter powers of 130W, 190W and 250W, respectively. This is because higher sputtering power gives off more material from the target.

Doping was found to cause a shift towards the visible wavelength range of the transmittance spectra as the doping was increased. This showed a shift in the absorption edge band that further showed a decrease in the bandgap when Nb doping is done on the pure TiO<sub>2</sub> films. Annealing of the films also caused a decrease in the bandgap this is because of the morphological dependency of the band gap on the annealing. This is because annealing changes the crystal structure of the TiO<sub>2</sub>.



The electrical results revealed that Nb doping of TiO<sub>2</sub> caused a decrease in the sheet resistance of the resultant films this implied there was improved electrical conductivity with an increase in the Nb doping content in TiO<sub>2</sub>. This was the same in the annealed samples, although the annealing caused a decrease in the sheet resistance of the same material films.

Gas sensing on the selected films revealed that the 4% Nb doped TiO<sub>2</sub> had the best hydrogen sensing profile with increasing sensitivity as the temperature was increased. The Pure TiO<sub>2</sub> and 2% Nb doped TiO<sub>2</sub> films tested for gas sensing showed that there was low sensitivity for the film to hydrogen gas supplied at 2000 ppm.

## **6.2 Recommendations**

There is a need to study the gas sensing properties of the Nb: TiO<sub>2</sub> at very low temperatures (less than room temperature) so as to determine if the material can sense gas leaks even at low temperatures since hydrogen fuel cells are being used as energy sources for cold storage rooms.

There is a need to look at the structural properties of Nb: TiO<sub>2</sub> to optimise structural orientation and phase transition of TiO<sub>2</sub> gives the optimal gas sensing properties which have not been covered in this study.

There is a need to build a complete prototype for the gas sensing device with all its circuit complete and thus advance field tests of the device in normal environmental conditions.

## REFERENCES

---

- Adawiya J., Raad M. and Khalied Z. (2011). Nanostructure dopants TiO<sub>2</sub> films for gas sensing, *Iraq journal of applied physics*, **7**(2), 1813-2065.
- Arndt M., Simon I., 2001, Hydrogen sensor for application in fuel cell vehicles. in: Proceeding of Sensor, 8-10 May 2001, *Nürnberg, Germany*, 541-545
- Arroyo, P., Meléndez, F., Suárez, J. I., Herrero, J. L., Rodríguez, S., and Lozano, J. (2020). Electronic Nose with Digital Gas Sensors Connected via Bluetooth to a Smartphone for Air Quality Measurements. *Sensors*, **20**(3), 786.
- Anukunprasert T., Saiwan C. Traversa E. (2005). The development of agas sensor for carbon monoxide monitoring using nanostructure of Nb:TiO<sub>2</sub>, *Science and technology of advanced materials*, **6**, 359-363.
- Ayadele A. D., Lasis E, U., Adeniyi Y. F., Joseph O. B., Kunle M. O., Samuel O. O. (2014). Electrical properties of Nano- TiO<sub>2</sub> thin film using spin coating method, *Journal of Materials and Material Characterization and Engineering*, **2**, 15-20.
- Azhar H., Jarmila P., Tomas P., Pavol D., Jan G., Martin T., Tomas R., Miroslav Z., Melinda V., Peter K., Anrej P. and Gustav P. (2012). Characterization and hydrogen gas sensing properties of TiO<sub>2</sub> Thin films prepared by Sol-Gel method, *Applied surface science*, **259**, 270-275.
- Banerjee, A. N. and K.K. Chatopadhyay (2005). Recent development in the field of crystalline P-type transparent conducting oxide thin films, *progress in crystal growth and characterization of materials*, **50**, 52-105.
- Bandgar, D. K., Navale, S. T., Khuspe, G. D., Pawar, S. A., Mulik, R. N., and Patil, V. B. (2014). Novel route for fabrication of nanostructured  $\alpha$ -Fe<sub>2</sub>O<sub>3</sub> gas sensor. *Materials science in semiconductor processing*, **17**, 67-73.
- Bedikyan L, Zacharieva S, and Zacharieva M (2013). Titanium Dioxide thin films, *Journal of chemical technology and metallurgy*, **48**(6), 555-558.
- Behzad koozegekaleji, RosoulSarraf-Mamoory, Akira Fujishima(2012). Influence of Nb dopant on the structural and optical properties of nanocrystalline TiO<sub>2</sub> thin films, *Material chemistry and physics*, **132**, 210-215
- Bihar, E., Deng, Y., Miyake, T., Saadaoui, M., Malliaras, G. G., andRolandi, M. (2016). A Disposable paper breathalyzer with an alcohol sensing organic electrochemical transistor. *Scientific reports*, **6**, 27582.
- Barnett, N. P., Celio, M. A., Tidey, J. W., Murphy, J. G., Colby, S. M., and Swift, R. M. (2017). A preliminary randomized controlled trial of contingency management for alcohol use reduction using a transdermal alcohol sensor. *Addiction*, **112**(6), 1025-1035.
- Bagolini, A., Gaiardo, A., Crivellari, M., Demenev, E., Bartali, R., Picciotto, A., and Bellutti, P. (2019). Development of MEMS MOS gas sensors with CMOS compatible PECVD inter-metal passivation. *Sensors and Actuators B: Chemical*, **292**, 225-232.

- Bie, L. J., Yan, X. N., Yin, J., Duan, Y. Q., and Yuan, Z. H. (2007). Nanopillar ZnO gas sensor for hydrogen and ethanol. *Sensors and Actuators B: Chemical*, **126**(2), 604-608.
- Boccuzzi F., Guglielmetti E. Chiorin A. (1992). IR study of gas- sensor materials by metals. *Sensors and Actuators B: Chemicals*, **7**(1-3), 645-650.
- Bochenkov V. E. and Sergeev G. B. (2010). Sensitivity, selectivity and stability of gas sensitive metal oxide nanostructures and their applications, *American scientific publishers, Russia*, **3**, 31-52.
- Brittan, W, H and Bardeen, J, (1953). Surface properties of Germanium, *Bell systems technical journal*, **32**, 1-4.
- Brown M., Jakeman (1996). Theory of 4- point probe technique as applied to film layer on conducting substrate, *British journal of applied physics*, **17**, 1146- 1149.
- Cai K., Hu Y., Jandt K. D. and Wang Y. (2008). Surface modification of TiO<sub>2</sub> Thin films with diffusion electrostatic self-assembly technique and its influence on osteoblast growth behaviour, *Journal of mater science; mater med*, **19**, 499-506.
- Chadwick, B., Tann, J., Brungs, M., and Gal, M. (1994). A hydrogen sensor based on the optical generation of surface plasmons in a palladium alloy. *Sensors and Actuators B: Chemical*, **17**(3), 215-220.
- Cheeke, J. D. N., and Wang, Z. (1999). Acoustic wave gas sensors. *Sensors and Actuators B: Chemical*, **59**(2-3), 146-153.
- Chengxiang Wang, Longwei Yin, Luyuan Zhang, Dong Xiang and Rui Gao (2010). Metal oxide gas sensors; Sensitivity and influencing factors, *sensors*, **10**, 2088-2106
- Chomkitichai W.,TamaekongN.,Liewhiran C.,Wisitsoraat A.,Sriwichai S.,and Phanichphant S. (2012). H<sub>2</sub>sensorbased onAu/TiO<sub>2</sub>nanoparticlessynthesizedbyflamespraypyrolysis,*Engineering Journal*,**16**(30),135–142.
- Claudio A., Donatella S., Giovanni N., Nicola D., Mariangela L., Rosalba P., Siglinda P. and Gabriele C. (2012). Development of hydrogen leak sensors for fuel cell transportation. *Chemical engineering transactions*, **26**, 333-338.
- Comini E., Fagilia G., Sberveglieri G., Li Y. X., Wlodarski W., Ghantashala M. K (2000). Sensitivity enhancement towards ethanol and methanol of TiO<sub>2</sub> films doped with Pt and Nb. *Sensors Actuators B: Chemical*, **64**, 169-174.
- Dakka A., Lafait J. Abd-Lafdil M. and Sella C. (1999). Optical study of Titanium Dioxide thin films prepared by RF sputtering, *MJ condensed matter*, **2**(1), 22-24.
- Davydovskaya, P., Pohle, R., Tawil, A., and Fleischer, M. (2013). Work function based gas sensing with Cu-BTC metal-organic framework for selective aldehyde detection. *Sensors and Actuators B: Chemical*, **187**, 142-146.

- De Marcellis, A., Ferri, G., and Mantenuto, P. (2013). Analog Wheatstone bridge-based automatic interface for grounded and floating wide-range resistive sensors. *Sensors and Actuators B: Chemical*, **187**, 371-378.
- Dey, A. (2018). Semiconductor metal oxide gas sensors: A review. *Materials Science and Engineering: B*, **229**, 206-217.
- Dler Adil (2019). Thin film deposition process, *International Journal of Modern Physics and Applications*, **1(4)**, 193-199
- Enrico Traversa, Maria Luisa Di Vona and Silva Licoccia, Michele Sacerdoti, Maria Cristina Carotta, Leugt Crema and Giuliano Martinelli (2001). Sol-gel TiO<sub>2</sub>- Based Nano-Sized powders for use in thick film gas sensors for atmospheric pollutants monitoring, *Journal of sol-gel science and Technology*, **22**, 167-179.
- Ferroni M., Carotta M., Guidi V., Martinelli G., Ronconi F., Sacerti M., and Traversa E. (2001). Preparation and characterization of nanosized Titania sensing film, *Sensors and Actuators B* **77**, 163-166.
- Fine, G. F., Cavanagh, L. M., Afonja, A., and Binions, R. (2010). Metal oxide semi-conductor gas sensors in environmental monitoring. *sensors*, **10(6)**, 5469-5502.
- Fujimoto M., Koyama H., Konagai M., Hosoi Y., Ishihara k., Ohnisi S and Awaya N (2006). TiO<sub>2</sub> anatase nanolayer on Tin thin film exhibiting high speed bipolar resistive switching. *Applied physics letters*, **89**, 223509-223509.
- Fujishima A. and Honda K. (1972). Electrochemical photolysis of water as a semiconductor electrode, *Nature*, **238**, 37-38.
- Ghenai, C., Salameh, T., and Merabet, A. (2020). Technico-economic analysis of off grid solar PV/Fuel cell energy system for residential community in desert region. *International Journal of Hydrogen Energy*, **45(20)**, 11460-11470.
- Ghosh, R., Gardner, J. W., and Guha, P. K. (2019). Air pollution monitoring using near room temperature resistive gas sensors: a review. *IEEE Transactions on Electron Devices*, **66(8)**, 3254-3264.
- Goto, T., Itoh, T., Akamatsu, T., Izu, N., and Shin, W. (2016). CO sensing properties of Au/SnO<sub>2</sub>-Co<sub>3</sub>O<sub>4</sub> catalysts on a micro thermoelectric gas sensor. *Sensors and Actuators B: Chemical*, **223**, 774-783.
- Gu, H., Wang, Z., and Hu, Y. (2012). Hydrogen gas sensors based on semiconductor oxide nanostructures. *Sensors*, **12(5)**, 5517-5550.
- Hasan.M., Haseeb A., Saidur R. and Masjuki H. (2008). Effects of post-annealing treatment on the optical properties of anatase TiO<sub>2</sub> thin films, *International scholarly and scientific research and innovation*, **2(4)**, 200-204
- Han, S. D. (2010). Review and new trends of hydrogen gas sensor technologies. *Journal of Sensor Science and Technology*, **19(2)**, 67-86.

- Han, C. H., Hong, D. W., Han, S. D., Gwak, J., and Singh, K. C. (2007). Catalytic combustion type hydrogen gas sensor using TiO<sub>2</sub> and UV-LED. *Sensors and Actuators B: Chemical*, **125**(1), 224-228.
- Hames, Y., Kaya, K., Baltacioglu, E., and Turksoy, A. (2018). Analysis of the control strategies for fuel saving in the hydrogen fuel cell vehicles. *International Journal of Hydrogen Energy*, **43**(23), 10810-10821.
- Haugen, J. E., Tomic, O., and Kvaal, K. (2000). A calibration method for handling the temporal drift of solid state gas-sensors. *Analytica chimica acta*, **407**(1-2), 23-39.
- Hench, L. L., and West, J. K. (1990). The sol-gel process. *Chemical reviews*, **90**(1), 33-72.
- Hotovy, I., Rehacek, V., Siciliano, P., Capone, S., and Spiess, L. (2002). Sensing characteristics of NiO thin films as NO<sub>2</sub> gas sensor. *Thin Solid Films*, **418**(1), 9-15.
- Hu, Y., Tan, O. K., Cao, W., and Zhu, W. (2004). A low temperature nano-structured SrTiO<sub>3</sub> thick film oxygen gas sensor. *Ceramics International*, **30**(7), 1819-1822.
- Huang S., Lin W. and Chen W. (2009). Gas sensitivity of indium oxide. *Trans. Nonferrous Met. Soc. of China*, **17**, 80-82.
- Jacobson, M. Z., Colella, W. G., and Golden, D. M. (2005). Cleaning the air and improving health with hydrogen fuel-cell vehicles. *Science*, **308**(5730), 1901-1905.
- Jakubik, W. P. (2011). Surface acoustic wave-based gas sensors. *Thin Solid Films*, **520**(3), 986-993.
- Kaiser, N. (2002). Review of the fundamentals of thin-film growth. *Applied optics*, **41**(16), 3053-3060.
- Karunagaran B. Kim K. Mangalaraj D., Yi J. and Veluman S. (2005). Structural, optical and Raman scattering studies on dc magnetron sputtered titanium dioxide thin films, *solar energy materials and solar cells*, **88**, 199-208.
- Kassa-Baghdouche, L. (2020). High-sensitivity spectroscopic gas sensor using optimized H1 photonic crystal microcavities. *JOSA B*, **37**(11), A277-A284.
- Kanaparthi, S., and Singh, S. G. (2020). Highly sensitive and ultra-fast responsive ammonia gas sensor based on 2D ZnO nanoflakes. *Materials Science for Energy Technologies*, **3**, 91-96.
- Kempster A. (1992). The principles and applications of chemical vapour deposition, *International Journal of Surface Engineering and Coating*, **70**(2), 68-75
- Kil Dong Lee (2005). Effect of substrate temperature on the optical and electrochromic properties of sputtered Ta<sub>2</sub>O<sub>5</sub> thin films, *Journal of the Korean Physical Society*, **46**(6), 1383-1391.
- Kington A. I., Maria J. P., and Straiffer S. K. (2000). Alternative electroluminescent to silicon dioxide for memory and logic devices. *Nature*, **406**(6799), 1032-1038.

- Korotcenkov, G. (2007). Metal oxides for solid-state gas sensors: What determines our choice?. *Materials Science and Engineering: B*, **139**(1), 1-23.
- Kumar, R., Al-Dossary, O., Kumar, G., and Umar, A. (2015). Zinc oxide nanostructures for NO<sub>2</sub> gas-sensor applications: A review. *Nano-Micro Letters*, **7**(2), 97-120.
- Lalchand A., Dirish N., Idrish G. and Dhanashri G. (2014). Nanocrystalline Pt-doped TiO<sub>2</sub> thin films prepared by spray pyrolysis for hydrogen gas detection. *Bull. Mater. Scie.* **37**(3), 425-432)
- Lee, J. M., Park, J. E., Kim, S., Kim, S., Lee, E., Kim, S. J., and Lee, W. (2010). Ultra-sensitive hydrogen gas sensors based on Pd-decorated tin dioxide nanostructures: Room temperature operating sensors. *international journal of hydrogen energy*, **35**(22), 12568-12573.
- Li, Z., Yao, Z., Haidry, A. A., Plecenik, T., Xie, L., Sun, L., and Fatima, Q. (2018). Resistive-type hydrogen gas sensor based on TiO<sub>2</sub>: A review. *International Journal of Hydrogen Energy*, **43**(45), 21114-21132.
- Lin H., Itsu C., Yang H., Lee P. and Yang C. (1994). Nanocrystalline WO<sub>3</sub>- based H<sub>2</sub>S sensor. *Sensors and Actuators B: Chemical*, **22**(1), 63-68.
- Liu, Y., Yu, J., and Lai, P. T. (2014). Investigation of WO<sub>3</sub>/ZnO thin-film heterojunction-based Schottky diodes for H<sub>2</sub> gas sensing. *International journal of hydrogen energy*, **39**(19), 10313-10319.
- Luther, B. P., Wolter, S. D., and Mohny, S. E. (1999). High temperature Pt Schottky diode gas sensors on n-type GaN. *Sensors and Actuators B: Chemical*, **56**(1-2), 164-168.
- Majumdar, S., Nag, P., and Devi, P. S. (2014). Enhanced performance of CNT/SnO<sub>2</sub> thick film gas sensors towards hydrogen. *Materials Chemistry and Physics*, **147**(1-2), 79-85.
- Mangrola M. H., Parmar B. H., Pillai A. S., and Joshi V. G.(2012), Structural, optical and electrical properties of TiO<sub>2</sub> Nanoparticles, *multi-disciplinary education Global Question*, **1**(1), 138-145.
- Moos R., Sahner K., Fleischer M., Guth U., Barsan N. and Weinar U. (2009). Solid state gas sensor research in German- a status report, *sensors*, **9**, 4323-4365.
- NaboruYamozoe (2005). Towards innovation of gas sensor technology. *Sensors and Actuators B: Chemical*, **108**, 2-14.
- Naji Al Dahoudi (2011). Low temperature gas coatings made through wet chemical Deposition of Niobium doped Titanium oxide colloid. *Material science and applications*, **2**, 265-269.
- Nasir, M. E., Dickson, W., Wurtz, G. A., Wardley, W. P., and Zayats, A. V. (2014). Hydrogen detected by the naked eye: optical hydrogen gas sensors based on core/shell plasmonic nanorod metamaterials. *Advanced Materials*, **26**(21), 3532-3537.
- Nazemi, H., Joseph, A., Park, J., and Emadi, A. (2019). Advanced micro-and nano-gas sensor technology: A review. *Sensors*, **19**(6), 1285.

- Novikov, S., Lebedeva, N., Satrapinski, A., Walden, J., Davydov, V., and Lebedev, A. (2016). Graphene based sensor for environmental monitoring of NO<sub>2</sub>. *Sensors and Actuators B: Chemical*, **236**, 1054-1060.
- Ogita, M., Higo, K., Nakanishi, Y., and Hatanaka, Y. (2001). Ga<sub>2</sub>O<sub>3</sub> thin film for oxygen sensor at high temperature. *Applied surface science*, **175**, 721-725.
- Olayinka O., Esther T., Oluseyi P., Stephine E. and Albert U. (2019). Overview of thin film deposition techniques. *AIMS Material science*, **6(2)**, 174-199.
- O'Leary S., Johnson S. and Lim P. (1997). The relationship between the distribution of electronic states and the optical absorption spectrum of an amorphous semiconductor, *J. Appl. Phys.*, **82**, 3334-3334.
- Oyabu Takashi (1982). Sensing characteristics of SnO<sub>2</sub> thin films gas sensor. *Journal of applied physics*, **53(4)**, 2785-2789.
- Prabir k. Mark Frank, Gary W. Hunter, Michael George (2005). Reactively sputtered Titania films as high-value carbon monoxide sensors, *sensor and actuators*, **B106**, 810-815.
- Prajapati, C. S., Soman, R., Rudraswamy, S. B., Nayak, M., and Bhat, N. (2017). Single chip gas sensor array for air quality monitoring. *Journal of Microelectromechanical Systems*, **26(2)**, 433-439.
- Pohle, R., Tawil, A., Davydovskaya, P., and Fleischer, M. (2011). Metal organic frameworks as promising high surface area material for work function gas sensors. *Procedia Engineering*, **25**, 108-111.
- Poloju, M., Jayababu, N., and Reddy, M. R. (2018). Improved gas sensing performance of Al doped ZnO/CuO nanocomposite based ammonia gas sensor. *Materials Science and Engineering: B*, **227**, 61-67.
- Raluca S., Miguel A., Edna J., Paul R., Mirium C., Jose A., Elson I. (2009). Grain size effect on the electrical response of SnO<sub>2</sub> Thin and thick film gas sensor, *Material research*, **12(1)**, 83-87.
- Rani, R. A., Zoolfakar, A. S., Ou, J. Z., Field, M. R., Austin, M., and Kalantar-zadeh, K. (2013). Nanoporous Nb<sub>2</sub>O<sub>5</sub> hydrogen gas sensor. *Sensors and Actuators B: Chemical*, **176**, 149-156.
- Reimer, L and Khol H. (2008). *Transmission Electron Microscopy: Physics of Image Formation*, 5<sup>th</sup> Edition, Springer.
- Rossi, M., and Brunelli, D. (2012, September). Ultra low power wireless gas sensor network for environmental monitoring applications. In *2012 IEEE Workshop on Environmental Energy and Structural Monitoring Systems (EESMS)* (pp. 75-81). IEEE.
- Rout, M., and Roy, R. (2016). Self-deployment of randomly scattered mobile sensors to achieve barrier coverage. *IEEE Sensors Journal*, **16(18)**, 6819-6820.
- Sato Y., Sanno Y., Tasaki C., Oka N., Kamiyama T., Shigesato Y. (2010). Electrical and optical properties of Nb-doped TiO<sub>2</sub> films deposited by dc magnetron sputtering using slightly

- reduced Nb-doped TiO<sub>2-x</sub> ceramic targets, *Journal of Vacuum Science and Technology a Vacuum Surface and Films*, **28**(4), 851-855.
- Sathish, V., Ramdass, A., Velayudham, M., Lu, K. L., Thanasekaran, P., and Rajagopal, S. (2017). Development of luminescent sensors based on transition metal complexes for the detection of nitroexplosives. *Dalton Transactions*, **46**(48), 16738-16769.
- Seiyama T., Kato A. Fujishi K and Nagatani M, (1962). A new detector for gaseous components using semiconductor thin films. *Analytical Chemistry*, **35**, 1502-1503.
- Sheilesh P., Manik C., Sanjay P., Bharat R., Dhanaji D., Pramod P., Shashwati S., Pradeep J., Vilcas P. (2011). Fabrication of Nanocrystalline TiO<sub>2</sub> thin films; Ammonia vapour sensor. *Journal of Sensor Technology*, **1**, 9-11.
- Shin, W., Matsumiya, M., Izu, N., and Murayama, N. (2003). Hydrogen-selective thermoelectric gas sensor. *Sensors and Actuators B: Chemical*, **93**(1-3), 304-308.
- Shin, W., Matsumiya, M., Qiu, F., Izu, N., and Murayama, N. (2004). Thermoelectric gas sensor for detection of high hydrogen concentration. *Sensors and Actuators B: Chemical*, **97**(2-3), 344-347.
- Schillini O. and Colbow K. (1994). A mechanism for sensing vanadium pentoxide films. *Sensors and Actuators B: Chemical*, **21**(2), 151-157.
- Song, P., Hu, J., Qin, H., Zhang, L., and An, K. (2004). Preparation and ethanol sensitivity of nanocrystalline La<sub>0.7</sub>Pb<sub>0.3</sub>FeO<sub>3</sub>-based gas sensor. *Materials letters*, **58**(21), 2610-2613.
- Suehiro, J., Hidaka, S. I., Yamane, S., and Imasaka, K. (2007). Fabrication of interfaces between carbon nanotubes and catalytic palladium using dielectrophoresis and its application to hydrogen gas sensor. *Sensors and Actuators B: Chemical*, **127**(2), 505-511.
- Sukon, P., Chalkaravin, L., Khatcharin, W., Anrant, W. and Adisorn T (2011). Flame-Made Nb-Doped TiO<sub>2</sub> Ethanol and Acetone sensors, *Sensors*, **11**, 472-484.
- Sun, D., Zhao, Y., Cao, Y., Liu, M., Zhang, Y., Zhao, L., Zhang, Y., Gao, J., Xu, C., Hao, T., Chen, J., and Ji, D(2020). Investigation on the Interaction Mechanism of the Solvent Extraction for Mercaptan Removal from Liquefied Petroleum Gas. *Energy & Fuels*, **34**(4), 4788-4798.
- Stamataki, M., Tsamakis, D., Brilis, N., Fasaki, I., Giannoudakos, A., and Kompitsas, M. (2008). Hydrogen gas sensors based on PLD grown NiO thin film structures. *Physica Status Solidi (a)*, **205**(8), 2064-2068.
- Thomas, G. W., Sousan, S., Tatum, M., Liu, X., Zuidema, C., Fitzpatrick, M., Koehler K.A., and Peters, T. M. (2018). Low-cost, distributed environmental monitors for factory worker health. *Sensors*, **18**(5), 1411.
- UyangaE., Gibaud A., Daniel P., Sangaa D., Savjidsuren G., Altantsong P., Bouvier T., Chih Haun Lee and Balagurov A. M. (2014). Structural and vibrational investigations of Nb-doped TiO<sub>2</sub> thin films, *Material Research Bulletin*, **60**, e222-e231



- Valencia S., Martin J. M. and Restepo G. (2012). Study of the band gap of synthesized titanium dioxide nanoparticles using the sol-gel method and a hydrothermal treatment, *The Open Material Science Journal*, **41**, 9-14.
- Vardan G., Elisabetta C., Guido F. and Giorgia S. (2013). TiO<sub>2</sub> Nanotubes; recent advances in synthesis and sensing properties, *Sensors*, **13**, 14813-14838.
- Van-Son D., Harish P., Jin H., Ke X., Nagendra B., Eugen E., Martina H., Andreas D., Teresa de Los A., Roland A. and Anjana D. (2014). Electrical and optical properties of TiO<sub>2</sub> thin films prepared by plasma enhanced atomic layer deposition, *Phys. Status Solidi A* **211(2)** 416-424.
- Vanotti, M., Blondeau-Patissier, V., Moutarlier, V., and Ballandras, S. (2015). Analysis of palladium and yttrium-palladium alloy layers used for hydrogen detection with SAW device. *Sensors and Actuators B: Chemical*, **217**, 30-35.
- Vellekoop, M. J. (1998). Acoustic wave sensors and their technology. *Ultrasonics*, **36(1-5)**, 7-14.
- Violeta Wichita, Joop Schoonman and Viorica Musat (2011). Ethanol and methanol sensing characteristics of Nb-doped TiO<sub>2</sub> porous thin films, *Physics Status Solidi A* **209**, 153-159.
- Wagner, C. (1950). The mechanism of the decomposition of nitrous oxide on zinc oxide as catalyst. *J. Chem. Phys*, **18**, 69-71.
- Wang, B., Zhu, L. F., Yang, Y. H., Xu, N. S., and Yang, G. W. (2008). Fabrication of a SnO<sub>2</sub> nanowire gas sensor and sensor performance for hydrogen. *The Journal of Physical Chemistry C*, **112(17)**, 6643-6647.
- Warren, B.E. (1990). *X-Ray Diffraction*, Dover publication, New York.
- Weast R. and Selby S. (1967). *Hand book of chemistry and physics CRC*, 3<sup>rd</sup> edition, 1245
- Wei-Cheng, Yu- Hsuan, Chao-Hao, Chun- Yen (2013). Sensing performance of precisely ordered TiO<sub>2</sub> nanowire gas sensor fabricated by electron- beam Lithography. *Sensors*, **13**, 865-874.
- Wei Z., Xinxin Z., Xinchon W., Luqi Y., Qiwei S. and Yuxing X. (2006). Structural and properties of Titanium oxide thin films deposited on unheated substrates at different total pressure by reactive dc magnetron sputtering with a substrate bias, *Journal of the Korean Physical Society*, **49(5)**, 2168-2175.
- Wen Z. and Tian-mo L. (2010). Hydrogen sensing characteristics and mechanism of nanosize TiO<sub>2</sub> doped with metallic ions, *Physica B*, **405**, 564-568.
- Wiebe, W., v Unwerth, T., and Schmitz, S. (2020). Using of an electrochemical compressor for hydrogen recirculation in fuel cell vehicles. *Fuel Cells*, **20(3)**, 362-369.
- Zhou, W., Apkarian, R., Wang, Z. L., and Joy, D. (2006). *Fundamentals of scanning electron microscopy (SEM)*. In *Scanning microscopy for nanotechnology* .1-40. Springer, New York, NY.

- Xu, Y., Yao, K., Zhou, X., and Cao, Q. (1993). Platinum-titania oxygen sensors and their sensing mechanisms. *Sensors and Actuators B: Chemical*, **14**(1-3), 492-494.
- Xu, K., Liao, N., Xue, W., and Zhou, H. (2020). First principles investigation on MoO<sub>3</sub> as room temperature and high temperature hydrogen gas sensor. *International Journal of Hydrogen Energy*, **45**(15), 9252-9259.
- Yang, Y., and Deng, Z. D. (2019). Stretchable sensors for environmental monitoring. *Applied Physics Reviews*, **6**(1), 011309.
- Yang, Z., Huang, Y., Chen, G., Guo, Z., Cheng, S., & Huang, S. (2009). Ethanol gas sensor based on Al-doped ZnO nanomaterial with many gas diffusing channels. *Sensors and Actuators B: Chemical*, **140**(2), 549-556.
- Yordanov R., Boyadjiev S., Georgieva V. (2014). Characterization of RF and DC magnetron reactive sputtered TiO<sub>2</sub> thin films for gas sensing. *Digest Journal of Nanomaterials and Biostructures*, **9**, 467-474.
- Yu J., Zhao X. and Zhao Q. (2000). Effect of surface structure on photocatalytic activity of TiO<sub>2</sub> thin films prepared by sol-gel method. *Thin solid films*, **379**, 7-14.
- Zhang, L., Tian, F. C., Peng, X. W., and Yin, X. (2014). A rapid discreteness correction scheme for reproducibility enhancement among a batch of MOS gas sensors. *Sensors and Actuators A: Physical*, **205**, 170-176.
- Zimmer, M., Burgmair, M., Scharnagl, K., Karthigeyan, A., Doll, T., and Eisele, I. (2001). Gold and platinum as ozone sensitive layer in work-function gas sensors. *Sensors and Actuators B: Chemical*, **80**(3), 174-178.
- Zhu, L., and Zeng, W. (2017). Room-temperature gas sensing of ZnO-based gas sensor: A review. *Sensors and Actuators A: Physical*, **267**, 242-261.